# Localization and distribution of nitric oxide synthase and other neuronal markers in the podia of *Holothuria arguinensis*.

**Nathalie Marquet[#], Adelino V.M. Canário and Deborah M. Power**

CCMAR Centre of Marine Sciences, University of Algarve, Campus de Gambelas, 8005-139 Faro, Portugal

[#]Corresponding author: N. Marquet

e-mail: <nmarquet@gmail.com>

Telephone: (351) 964390335

Fax: (351) 289 818 353

Email of the other authors:

Adelino V.M. Canário: acanario@ualg.pt

Deborah M. Power: dpower@ualg.pt

## Abstract

The organization of the nervous system of the holothurian podia – the tentacles, papillae, and tube feet – is still poorly understood which limits the development of functional studies. Knowledge about nitric oxide (NO) signalling in sea cucumber is non-existent, although it is known to play an important role in many essential biological functions, including neurotransmission, throughout the Animal Kingdom. The objective of this study was to characterize the holothurian podia in *Holothuria arguinensis* using classical histology, nitric oxide synthase (NOS) distribution using NADPH diaphorase histochemistry and NOS immunostaining, and neuronal immunohistochemistry. Our results revealed an abundant distribution of NO in the nervous components of the holothurian podia, suggesting an important role for NO as neuronal messenger in these structures. Nitrergic fibres were intensively labelled in the longitudinal nerve and the nerve plexus surrounding the stem and had a weaker signal in the mesothelium. NOS was also found in scattered cells bodies and abundant fibres in the disc, with evident neuronal projections to the bud surface, especially in the tentacles. The disc was the most specialized area and was characterized by a specific nervous arrangement, consisting of a distinct nerve plate, rich in cells and fibres containing potential sensory cells staining positively for neuronal markers, which makes this region the most seemingly chemosensory candidate for future exploration.



**Key words**: histology, immunohistochemistry, NADPH-diaphorase, nitric oxide, sea cucumber

# 1. Introduction

Echinoderms are slow-moving and mostly broadcast spawning marine invertebrates that have very limited or a total lack of vision and audition. Although they react to light and touch (e.g. Ullrich-Lüter, Dupont, Arboleda, Hausen, & Arnone, 2011; VandenSpiegel, Flammang, Fourmeau, & Jangoux, 1995), chemical cues are proposed to be crucial for survival and reproduction. (e.g. Ullrich-Lüter et al., 2011; VandenSpiegel et al., 1995). This idea is supported by numerous studies demonstrating that they perceive and respond to waterborne stimuli from predators, damaged conspecifics, potential food sources and conspecific mates (e.g. Caballes & Pratchett, 2017; Campbell, Coppard, D'Abreo, & Tudor-Thomas, 2001; Cyrus, Bolton, Scholtz, & Macey, 2015; Dix, 1969; Hamel & Mercier, 1996; Mann, Wright, Welsford, & Hatfield, 1984; Marquet, Hubbard, da Silva, Afonso, & Canário, 2018; Soong, Chang, & Chao, 2005; Unger & Lott, 1994). However, the sensory structures involved in the detection of chemical cues have not yet been identified. This is partly due to the difficulty in performing electrophysiological assays as a consequence of: 1) the small size of nerve cells and the organisms hard protective calcareous endoskeleton (Cobb, 1978; Pentreath & Cobb, 1972), and 2) the lack of knowledge about the nervous system of adult echinoderms, mostly due to the shortage of molecular markers to clearly identify neurons (Díaz-Balzac, Vázquez-Figueroa, & García-Arrarás, 2014).

Sea cucumbers are soft bodied and worm-like echinoderms that have as the main body wall structures: tube-feet, papillae and tentacles. These represent the three types of holothurian podia and they are all connected to the water-vascular system and the integument. They are composed of a stem and a disc, forming a functional unit, and are characterized by four tissue layers typically seen in echinoderm podia: an inner mesothelium, a connective tissue layer, a nerve plexus and an outer epidermis covered by a well-defined cuticle (Fig. 11A) (e.g. Cavey, 2006; Flammang, Ridder, & Jangoux, 1991; Santos, Haesaerts, Jangoux, & Flammang, 2005;

VandenSpiegel et al., 1995). Due to their direct contact with the environment, they are good candidate structures for the perception of environmental stimuli. The podia are proposed to have a sensory role (Bouland, Massin, & Jangoux, 1982; Hyman, 1955; Pentreath & Cobb, 1972; VandenSpiegel et al., 1995) although, so far, the functional organization of their nervous tissue has been much less studied than the radial nerve cords (RNCs) (for summary, see Díaz-Balzac, Lazaro-Pena, Vazquez-Figueroa, Diaz-Balzac, & Garcia-Arraras, 2016), the principal structure of the echinoderm nervous system (Cobb, 1987; Hyman, 1955). Until recently, almost all knowledge of the nervous system of echinoderms was based on classical histology carried out early during the last century and, more recently, on electron microscopy studies (e.g. Bouland et al., 1982; Cavey, 2006; Flammang & Jangoux, 1992; Hyman, 1955; McKenzie, 1987; Pentreath & Cobb, 1972; VandenSpiegel et al., 1995). With the development of new neural markers, neuronal and fibre populations expressing different neurotransmitters, such as catecholamines and neuropeptides, have been identified, contributing to a more comprehensive view of the echinoderm nervous system (Díaz-Balzac, Abreu-Arbelo, & García-Arrarás, 2010; Díaz-Balzac & García-Arrarás, 2018; Díaz-Balzac, Mejías, Jiménez, & García-Arrarás, 2010; Díaz-Balzac et al., 2007; Díaz-Balzac et al., 2014; Díaz-Miranda, Blanco, & Garcia-Arraras, 1995; Hoekstra, Moroz, & Heyland, 2012; Inoue, Tamori, & Motokawa, 2002).

Nitric oxide (NO) is synthesised from L-arginine by the NADPH-dependent enzyme nitric oxide synthase (NOS), and is involved in many essential biological functions including immune defence, vascular regulation, muscle relaxation and, not least, neuromodulation and neurotransmission (Colasanti & Venturini, 1998; Moncada, Palmer, & Higgs, 1991; Palumbo, 2005; Snyder & Bredt, 1991). NOS is found throughout the Animal Kingdom from mammals to invertebrates and its amino acid sequence is relatively well conserved in the different phyla studied so far (Martínez, 1995; Palumbo, 2005). This suggests that NO signalling is an ancient

system that has been retained during evolution due to the high adaptive value it confers (Jacklet, 1997).

The peripheral and central nervous systems in invertebrates are the most reported sites for the production of NO (Martínez, 1995) and NOS activity has been found in the nerves of chemosensory organs from many invertebrates such as molluscs (Elofsson, Carlberg, Moroz, Nezlin, & Sakharov, 1993; Moroz, 2006; Moroz et al., 1994), jellyfish (Moroz, Meech, Sweedler, & Mackie, 2004), crustaceans (Talavera et al., 1995) and insects (Elphick, Green, & O'Shea, 1994; Müller, 1997; Villar, Settembrini, Hokfelt, & Tramezzani, 1994). In some species, biochemical and physiological analyses have demonstrated the role of NO in olfaction (see review Johansson & Carlberg, 1995). In adult echinoderms, NOS was reported in the starfish cardiac stomach (Martínez, Riveros-Moreno, Polak, Moncada, & Sesma, 1994) and NO was shown to regulate its contractility (Elphick & Melarange, 1998). However, nothing is currently known about the presence, distribution and role of NOS in putative chemosensory podia of echinoderms.

In sea cucumbers, cells with morphological characteristics typical of sensory cells have been described in the tentacles, tube feet and papillae (Bouland et al., 1982; Flammang & Jangoux, 1992; VandenSpiegel et al., 1995). They were characterized as ciliated cells bearing a short and non-motile cilium and ending within the nerve plexus, which is considered a diagnostic feature of sensory cells (Holland, 1984). More recently, sensory-like cells were described using immunohistochemistry and they were characterized by their distinct bipolar organization and apical processes which extended towards the epithelial surface. In some cases, glomeruli-like structures, potential sites of dense synaptic connection, were found below the cell bodies (Díaz-Balzac, Abreu-Arbelo, et al., 2010; Hoekstra et al., 2012).

Despite recent progress in mapping the nervous system of sea cucumbers, the diversity of species, their enigmatic behaviour and the absence of clearly identified sensory cells and

neural circuits, make more studies essential. In particular, characterization of the distribution of neurotransmitters and other neuronal pathways will help to improve understanding of the function of different sensory structures in sea cucumbers. The present study was performed to characterize the morphology of the main tissues in contact with the environment, namely the tentacles, tube feet and papillae, in the sea cucumber *Holothuria arguinensis.* The morphology of these tissues was studied using 1) classical histological methods to describe tissue organization and confirm previous findings, 2) NADPH-diaphorase histochemistry and NOS immunohistochemistry and 3) immunohistochemistry using antibodies against β-tubulin (a neuronal marker) and serotonin (a neurotransmitter).

## 2. Methods

### 2.1.Ethics statement

Sea cucumbers, *Holothuria arguinensis* KOEHLER & VANEY 1906 (Holothuroidea, Aspidochirotida) were collected, handled and euthanized in agreement with the license N° 635/2015/CAPT and N°95/2016/CAPT of the ICNF - Instituto da Conservação da Natureza e das Florestas, Portugal. The species is not endangered nor protected.

### 2.2.Animals

Adult *H. arguinensis* (>210 mm length) were collected in the intertidal zone of the Ria Formosa (37°00’35.02’’N) in Faro (Portugal). They were kept at Ramalhete Marine Station and fed with sediment collected from their natural environment.

### 2.3.Morphology

The entire animal and the structures of interest (Figs. 1A, B) were initially observed using an Olympus SZ-PT binocular microscope coupled to an Olympus SC35 camera. The external anatomy of *H. arguinensis* was photographed and studied in detail, and a diagram was rendered in Adobe Illustrator by Scigrades (https://scigrades.be).

### 2.4.Tissue sampling

120 Sea cucumbers were anesthetized with 5% $MgCl_2$ (Sigma, St. Louis, MO, USA) before
121 tissue collection. Samples of the tube feet, tentacles and papillae and the body wall including
122 the radial nerve cord (RNC; as staining control) were dissected out from the anterior, middle
123 and posterior regions and fixed in 4% paraformaldehyde at 4°C for 1 to 24 h depending on the
124 subsequent procedure. After fixation, samples were rinsed three times in 0.1 M phosphate-
125 buffered saline (PBS) for 15 min and stored either in 70% ethanol for histology or sucrose for
126 histochemistry and immunohistochemistry.

127 **2.5.Histology**

128 For standard histology, tissue samples were dehydrated in a graded sequence of ethanol
129 (from 70% to 100%), saturated in xylene and embedded in paraffin wax (Merck, Germany).
130 Serial sections (8 µm) were cut with a rotary microtome (Leica RM2135) and mounted on poly-
131 L-lysine coated slides. Sections were dewaxed in xylene and then rehydrated in a decreasing
132 alcohol series (100 to 70%). To characterize the general tissue organization several stains were
133 used: Alizarin Red S (Sigma-Aldrich, St. Louis, MO, USA) to stain calcium deposits, Masson's
134 trichrome (MT) or Milligan's trichrome (MiT) to distinguish tissue, and Palmgren's silver stain
135 to localize nerve fibres (Humason, 1972). MT stains the collagen fibres green, nuclei pink,
136 muscle cells red and nerve fibres light red. With MiT, collagen fibres are blue, nuclei and
137 muscle cells are magenta and nerve fibres purple. Palmgren's silver stains nerves dark brown
138 or black while the background appears light brown. After staining, sections were rapidly
139 dehydrated through an alcohol series (70% to 100%), cleared in xylene and mounted in DPX
140 (BioChemika, Sigma-Aldrich, Madrid, Spain) and covered with a glass coverslip.

231 **2.6.Histochemistry**

232 For NADPH diaphorase (NADPH-d) histochemistry, the tissue samples were
233 cryoprotected with a graded series of sucrose (10 to 30%) and frozen into Tissue-Tek (Sakura
234 Finetek, Torrance, CA) using a dry-ice and ethanol mixture. Serial sections of 20 µm were

prepared with a cryostat (NX50 cryostat, Thermo Scientific, Waltham, MA, USA), mounted on 3-aminopropyltriethoxysilane (APES; Sigma-Aldrich, Madrid, Spain) coated glass slides and stored at -25°C. When needed, the slides were brought to room temperature and washed three times for 15 min in 0.2 M Tris-HCl before NADPH-d staining as described by Elphick (1997). Slides were immersed in the staining solution and kept in the dark for at least three hours: 1 mM NADPH (TetraTris salt), 0.5 mM nitroblue tetrazolium (NBT), and 0.5 % Triton X-100 in 0.2 M Tris-HCl at pH 8.0. Post-staining preparations were washed three times for 10 min in Tris-HCl before mounting in glycerol gelatine (Sigma-Aldrich, GG1, Madrid, Spain). The intensity of NADPH-d staining is correlated to the biochemical activity of NOS (Elofsson et al., 1993). Histochemical controls omitted the NADPH from the staining solution and in this case no specific stain was observed.

**2.7.Immunohistochemistry**

Frozen sections were prepared as described in Section 2.6. The slides were washed three times for 15 min in PBS and blocked for 3 hours in Tris-carrageenan Triton X-100 (TCT, Tris buffer containing 0.7% carrageenan and 0.5% Triton X-100, pH 7.6) blocking solution containing 3% sheep serum (Sigma-Aldrich, Madrid, Spain). The primary antibodies chosen to characterize the neural structures in sea cucumbers were against: (1) serotonin, a widely distributed neurotransmitter in the central and peripheral nervous system in vertebrates and invertebrates (Gillette, 2006) and (2) β-tubulin, a building block of microtubules which are abundant in neurons. The primary antibodies used were anti-NOS universal (Sigma, N-217; Lot. SLBQ488V) at a dilution of 1:100, the anti-β-tubulin (Sigma, T-4026; Lot. 107M4801V) at a dilution of 1:250, and the anti-serotonin (Sigma, S-5545; Lot. 025M4792V) at a dilution of 1:400 (Table 1). Primary antibodies were incubated with tissue sections overnight at 4°C and optimal dilutions were identified by testing serial dilutions on tissue sections and selecting those that gave the best signal to noise ratio. The anti-serotonin and anti-tubulin antibodies used in

this study have previously been used in other species of sea cucumbers and their specificity demonstrated (Díaz-Balzac, Abreu-Arbelo, et al., 2010; Díaz-Balzac et al., 2016; Díaz-Balzac et al., 2007; Inoue et al., 2002; Nakano, Murabe, Amemiya, & Nakajima, 2006; Tamori et al., 2007). After incubating with the primary antibodies and rinsing twice for 5 min in PBS, the slides were incubated with the secondary antibodies diluted in PBS for two hours at room temperature. The secondary antibodies used were Alexa Fluor 546 conjugated anti-mouse IgG (Molecular Probes, Eugen, Oregon; A-11030) at a dilution of 1:400 for the anti-tubulin antibody and Alexa Fluor 546 conjugated anti-rabbit IgG (Molecular Probes, Eugen, Oregon; A-11035) at a dilution of 1:400 for the anti-serotonin and anti-NOS antibodies. Antibodies were applied separately on serial tissue sections as co-localization studies could not be performed due to the presence of tissue autofluorescence under the GFP filter (green). Cell nuclei were stained with DAPI (Sigma, St. Louis, MO, USA) at a dilution of 1:20000 for 5 min. After washing in PBS, the sections were mounted in glycerol gelatine (Sigma-Aldrich, GG1, Madrid, Spain). Negative control slides included omission of the primary antibodies, omission of both primary and secondary antibodies and showed little or no labelling of the tissue sections.

### 2.8.Imaging

Stained sections from histology were analysed using light or fluorescence microscopy and a Zeiss Axioimager Z2 (Carl Zeiss Group) coupled to a digital camera (Axiocam ICC3) linked to a computer for digital image analysis. Image processing, including brightness/contrast adjustments, were performed within ImageJ Fiji (http://imagej.net/Fiji).

## 3. Results

### 3.1.Morphology

*H. arguinensis* has, in common with other sea cucumbers, an elongated cylindrical shaped body, with a mouth (anterior part, A) and an anus (posterior part, P) at the opposite extremities of the central body axis (Fig. 1A). The body is covered by tube feet, or locomotor

podia, on both ventral (V) and dorsal (D) sides, although they are more abundant on the ventral side. The dorsal side is darker and harder than the ventral side, and possesses papillae, or non-locomotor podia, arranged in four rows. An additional two rows of papillae are located laterally between the ventral and dorsal sides. The oral cavity contains the mouth surrounded by 20 peltate tentacles (*i.e.* buccal podia; cauliflower-like in appearance), although 19 and 21 tentacles were counted in some individuals (Fig. 1B). The tentacles, tube feet and papillae are protrusions of the body wall and are associated with the water-vascular system. Each of these appendages is composed of a proximal stem and a distal disc (tentacles and tube feet) or pointed conical structure (papillae); however, the tissue organization of each appendage has distinguishing characteristics (see below). To assess the specificity of the histological staining and antibodies used in the study, they were also applied to sections of the better characterized RNCs and the results can be seen in supporting information Figs. S1 and S2.

### **3.2**. **Tentacles**

In *H. arguinensis*, the stem of the tentacles was cylindrical and topped by a disc with a cauliflower shape (Fig. 2A). The stem was subdivided into 5-10 secondary branches from which 3-5 tertiary branches extended and ended in a rounded papilla. Each papilla was itself composed of 2 to 5 buds (Fig. 2B).

#### *3.2.1. Tissue organization*

The MT and Palmgren positive tissues in the stem and the bud of the tentacles were the cuticle, epidermis, outer connective tissue (including central and external connective tissue), buccal or tentacular nerve, inner connective tissue and mesothelium (Figs. 2B, C, D). At the centre of each tentacle, the ambulacral lumen, which is a continuation of the water-vascular canal system, was visible. Calcareous ossicles, identified as black deposits with Palmgren staining and Alizarin red positive (not shown), were seen in the central connective tissue of the stem (Fig. 2D). However, they were never seen in the bud of the tentacles. Palmgren's staining

revealed the proximity of the buccal nerve to the connective tissue layer in both parts of the tentacle (Fig. 2D). Peripheral neurites were clearly seen in the mesothelium within the stem (Fig. 2E) and in the bud where they formed apical neurites scattered among the epidermal cells and in the nerve plate (Fig. 2F). MiT revealed the buccal nerve plexus which formed a cylindrical meshwork and was asymmetrically thickened to form a longitudinal buccal nerve (Fig. 2G). The latter ran longitudinally on one side of the cylinder.

*3.2.2. Localization and distribution of nitric oxide synthase*

The NADPH-d staining and the anti-NOS antibody showed an overall similar distribution in the tentacle. In the stem (Figs. 3A, B), the longitudinal buccal nerve (Figs. 3C, D) and the buccal nerve (Figs. 3E, F) were strongly reactive to both markers. The mesothelium was also positive for NADPH-d and anti-NOS (Figs. 3E, F). In the bud, NOS was revealed by the two methods in both the buccal nerve and mesothelium (Figs. 3G, H). Interestingly, many nerve fibres were seen in the bud epidermis and the signal was particularly intense with the anti-NOS method. Numerous nitrergic fibres were also identified in the nerve plate (Figs. 3I, J). Nitrergic cell bodies were seen in this area with both methods used (Figs. 3J, K), and elongated oval cells with neuronal projections were clearly identified with the anti-NOS sera (Fig. 3K). Control sections are presented in supporting information Figs. S3 and S4.

*3.2.3. Comparison with the other neuronal markers*

The three markers, anti-NOS, anti-serotonin and anti-tubulin, labelled the interior of the main nervous structures (buccal nerve and nerve plate) in the bud of the tentacle (Figs. 4A, B, C). The disc of the tentacle had many nitrergic fibres between the epidermal cells, some extending to the surface of the bud, and they were also observed in the nerve plate and buccal nerve (Fig. 4A). A few serotonin-positive cell bodies were evident amongst the epidermal cells and positive serotonergic fibres were seen in the nerve plate and buccal nerve (Fig. 4B). Fibres within the disc and the nerve plate were positive for anti-tubulin (Fig. 4C). DAPI staining

361 revealed the cell nuclei of the abundant epidermal cells of the bud (Fig. 4D). Negative controls
362 are presented in supporting information Fig. S5.

363 **3.3. Tube feet**

364 The tube feet in *H. arguinensis* had the same external morphology regardless of their
365 position in the body and belonged to the disc-ending group of podia and were characterized by
366 a basal cylindrical stem topped by a flattened disc (Fig. 5A).

367 *3.3.1. Tissue organization*

368 MiT staining revealed no differences in the tissue layers of the dorsal and ventral tube
369 feet. They were all composed of a cuticle, epidermis, connective tissue (external and central),
370 podial nerve, connective tissue (internal) and mesothelium (Fig. 5B). The tube feet had a
371 terminal disc in which two clusters of cells could be seen: one composed of densely packed
372 epidermal cells at the tip of the disc (outer cell cluster) and another composed of loosely packed
373 cells at the bottom of the disc (inner cell cluster). Connective tissue was seen between the two
374 groups of cells and on the top of the inner cell cluster, where it stained most intensely (Fig. 5C).
375 As in the tentacle, the nervous tissue consisted of a podial nerve plexus that was enlarged
376 asymmetrically to form the longitudinal podial nerve (Fig. 5D). Nerve fibres were identified
377 with Palmgren's staining within the terminal disc and in the podial nerve plexus of the stem,
378 although the staining was masked, to some extent, by the general brown coloration of the tube
379 feet and the black deposits in the calcium rich areas (Fig. 5E). In contrast to the observations in
380 the tentacles, alizarin red staining showed that the calcareous ossicles were only present on the
381 outer proximal surface of the terminal disc of the tube feet, as a support for the disc (Fig. 5F).

382 *3.3.2. Localization and distribution of the nitric oxide synthase*

383 The NADPH-d staining and the anti-NOS antibody were positive in the podial nerve
384 plexus, in the mesothelium and connective tissue (Figs. 6A, B). Nitrergic fibres were clearly
385 evident in the podial nerve plexus and in the mesothelium (Figs. 6C, D, E). In the distal disc,

386 the NADPH-d and anti-NOS reactivity were more diffuse than in the stem although weakly
387 reactive fibres could be distinguished separating the two cell clusters, indicating most likely the
388 localization of the nerve plate (Fig. 6F, G). In addition, NOS-positive cell bodies were seen in
389 the disc in close proximity to the nerve plate (Fig. 6H). Negative controls for NADPH-d staining
390 and anti-NOS sera are presented in supporting information Fig. S6.

391 *3.3.3. Comparison with the other neuronal markers*

392 The anti-tubulin, anti-serotonin and anti-NOS were immunoreactive with fibres in the
393 nerve plate of the disc, which was located between the inner and outer cell cluster of the disc
394 (Figs. 7A - C). Fibres immunoreactive to anti-NOS (Fig. 7A) and anti-serotonin (Fig. 7B) were
395 detected in the two cell clusters (outer and inner clusters) and some projected directly from the
396 nerve plate. However, they were much less abundant than the fibres immunoreactive with anti-
397 tubulin (Fig. 7C). Immunoreactive cell bodies were scarce although some nitrergic and
398 serotonergic immunoreactive cells were seen in proximity to the nerve plate (Figs. 7A, B). The
399 disc was highly cellular as shown by the abundant DAPI staining of the nuclei of the inner and
400 outer cell clusters (Fig. 7D).

401 The anti-tubulin, anti-serotonin and anti-NOS immunoreactivity in the stem of the tube
402 feet was identical to that seen in the stem of the papillae and tentacles. All the nervous elements
403 in the stem of the three different appendages (tube feet, papillae, tentacles) were
404 immunoreactive with anti-tubulin, anti-serotonin and anti-NOS. The immunoreactivity of
405 nitrergic fibres was strong in the podial nerve plexus while the signal was weaker in the
406 connective tissue and the mesothelium (Fig. 7E). The same pattern of immunoreactivity was
407 obtained with the anti-tubulin antibody (Fig. 7G). A few anti-serotonin and anti-NOS
408 immunoreactive cell bodies were observed in the podial nerve plexus along with occasional
409 immunoreactive nerve fibres (Figs. 7E, F). DAPI-stained sections showed an abundance of cell
410 nuclei in the mesothelium and podial nerve plexus while there were fewer nuclei in the

connective tissue (Fig. 7H). Negative controls are presented in supporting information Figs. S7 and S8.

### 3.4.Papillae

Papillae are conical appendages that have a cylindrical pigmented stem surmonted by a whitish prominence evident as a conical pointed structure (Fig. 8A).

#### *3.4.1.Tissue organization*

Alizarin red staining revealed that papillae contained calcareous ossicles in the upper part, lining the proximal terminal end, as observed in the tube feet (Fig. 8B). MiT staining showed that the stem was mainly composed of a dense network of connective tissue in which an ambulacral lumen communicated with the water-vascular system. From the interior to the surface of the stem, four tissue layers could be seen: the mesothelium, a thin layer of connective tissue and the podial nerve plexus (confirmed with Palmgren's staining) and an outer layer of connective tissue (Fig. 8C). As for the tentacle and the tube feet, the papillae nervous tissue contained a longitudinal papillae nerve that ran on one side of the papillae and was surrounded by nerves with an organisation consistent with a nervous plexus. The pointed structure of the papillae was dense in cells and was supported by ossicles as shown by the H&E staining (Fig. 8D). Palmgren's staining showed numerous nerve fibres in the terminal end of the papillae (Fig. 8E).

#### *3.4.2. Localization and distribution of nitric oxide synthase*

As seen in the histology, ossicles are found just below the terminal end of the papillae (Fig. 9A). In this area, fibres and a number of cell bodies (< 10 µm in diameter) were immunoreactive with anti-NOS (Fig. 9B). The NADPH-d staining in this region was more diffuse and highlighted many nitrergic fibres (Fig. 9C). In the stem, immunoreactivity with anti-NOS (Figs. 9D, E) and NADPH-d staining (Fig. 9F) were seen in the papillae nerve, the connective tissue and the mesothelium where fibres and cell bodies could be seen. Negative

controls for NADPH-d staining and anti-NOS sera are presented in supporting information Figs. S9 and S10.

*3.4.3. Comparison with the other neuronal markers*

In contrast to the tube feet but in common with the tentacle, the terminal end of the papillae was composed of only one group of cells. Nitrergic and serotonergic cell bodies were seen in very low abundance scattered amongst the epidermal cells (Figs. 10A, B). As for the tentacles and tube feet, anti-NOS (Fig. 10A) and anti-tubulin (Fig. 10C) immunoreactive nerve fibres were clearly distinguishable between the epidermal cells. The DAPI-stained section revealed a highly cellular disc in the papillae (Fig. 10D). Negative controls are presented in supporting information Fig. S11.

# 4. Discussion

This study revealed abundant distribution of NOS in the nervous components of the podia, in both stem and disc (i.e., discs in tentacle and tube feet and pointed conical structure in papillae), which suggests NO may be an important neuronal messenger in sea cucumbers. Our results indicated that the disc is the most specialized area of the podia characterized by 1) groups of cells arranged differently between type of podia, some of which stained with neuronal markers suggesting they could be sensory neurons and 2) a specific nervous arrangement with a distinct nerve plate from which nerve fibres extended into the disc. The podial disc may be a promising candidate for future functional studies directed at identifying chemosensory structures and the signalling compounds they detect. The findings of this study are summarized in Figure 11.

## 4.1.Localization of the nervous system

For simplicity, the terminology has been maintained throughout the text; i.e., the disc of the tentacle and tube feet and the conical structure of the papillae. The tissue stratification of the tentacle, tube feet and papillae were characteristic of an echinoderm podia (Fig. 11A) (see

review Flammang, 1996). However, the tissue layer organization and the cell and fibre composition differed depending on whether they belonged to the stem or the disc of the podia (see below). The main nervous system of the podia had an appearance consistent with a nerve plexus that surrounded the stem (or fenestrated sheath), and which was asymmetrically thickened to form the longitudinal nerve. As in other Holothuroidea, it was located in the deeper part of the connective tissue close to the mesothelium, although there was a thin layer of connective tissue between the two (Díaz-Balzac, Abreu-Arbelo, et al., 2010; Flammang & Jangoux, 1992). This is in contrast, to other echinoderms in which the nerve plexus lies just beneath the epidermis (Florey & Cahill, 1977; Moore & Thorndyke, 1993). This difference has been related to the thickness of the connective tissue (Díaz-Balzac, Abreu-Arbelo, et al., 2010).

**4.2.Nitric oxide synthase**

The scarce studies available in echinoderm show NOS in the eggs (Leckie et al., 2003) and ciliary band of sea urchin larvae (Bishop & Brandhorst, 2007) and in the starfish neuroendocrine system (Martínez et al., 1994) and coelomocytes (Beck et al., 2001). In the current study, NOS distribution was demonstrated for the first time in a sea cucumber and shown to be widespread in the three types of holothurian podia, underlining the importance of NO in sea cucumber biology.

The two methods for NOS detection, NADPH-diaphorase staining and anti-NOS immunohistochemistry, have been shown to give consistent results in many species (e.g. Dawson, Bredt, Fotuhi, Hwang, & Snyder, 1991; Hope, Michael, Knigge, & Vincent, 1991; Meulemans et al., 1995; Nacsa, Elekes, & Serfőző, 2015). The occasional discrepancies found in NOS detection between the two approaches have been attributed to the lower specificity of the NADPH-diaphorase method (Bruning, 1994; Holmqvist, Ostholm, Alm, & Ekstrom, 1994) or the lack of specificity of antisera raised against mammalian NOS when used in invertebrates due to the low sequence conservation of the protein (Cooke, Edwards, & Anderson, 1994;

Moroz et al., 1994). In our study, the two methods used to detect NOS gave consistent results, although it is recommended as a precaution to use both methods if a species-specific antiserum is not available. Nevertheless, the mammalian anti-NOS serum used in our study was immunoreactive with the sea cucumber NOS, which is unsurprising when the amino acid sequence conservation of the enzyme between sea cucumbers and mammals is taken into account (Martínez et al., 1994; Palumbo, 2005). NOS was widespread in both stem and disc of all three types of podia and in their different constitutive tissues (i.e., connective and nervous tissue, mesothelium) (Figs. 11B-E). The role of NO in echinoderms has been little studied but includes metamorphosis, fertilization and muscle relaxation (Bishop & Brandhorst, 2007; Elphick & Melarange, 1998; Leckie et al., 2003). In the present study, NOS was most abundant in the stem nervous system, including the longitudinal nerve and putative nerve plexus (Fig. 11B). This suggests an important role for NO in the nervous system of sea cucumbers. Taking into consideration the large extension of NO positive fibres in the nerve plexus and the mesothelium within the stem, it is particularly tempting to suggest that NO might be involved in the motor activity of the podia, such as has been described in stomach relaxation of the starfish *Marthasterias glacialis* (Elphick & Melarange, 1998; Martínez, 1995; Martínez et al., 1994). A subtler modulatory or sensory function, nevertheless, should not be excluded.

In addition to its presence in the stem of the podia, NOS was also detected in scattered cell bodies and abundant fibres in the disc, where the NADPH-d staining appeared to be less intense and more diffuse than in the stem (Figs. 11C-E). Some cells with their apical projections to the bud surface were particularly obvious, notably in the tentacle bud. The disc has been reported to have the characteristics of a sensory structure (Bouland et al., 1982; Flammang & Jangoux, 1992; VandenSpiegel et al., 1995), raising the possibility that one of the possible roles of NO in this area could be sensory perception. In other taxa, such as molluscs, insects and mammals, NO has been described as a modulator of chemosensory processing, in which NOS

511 was seen to be highly selective and abundant in chemosensory areas (e.g. Breer & Shepherd,
512 1993; Elphick et al., 1994; Gelperin, 1994; Moroz, 2006). However, to address the functional
513 role of NO in sensory perception and particularly in chemoreception in sea cucumbers, further
514 studies are required.

515 **4.3.Disc innervation**

516 The disc of the podia was clearly different from the stem and was the most specialized
517 part in all three types of podia. It was a more cell rich structure than the stem, which had scarce
518 DAPI nuclear staining, and the organization of the cells differed according to the type of podia.
519 The disc of the tube feet and the conical structure of the papillae consisted of a single surface;
520 this was separated into two cell groups in the tube feet, while only one cell group was seen in
521 the papillae. In contrast, the tentacles presented several buds containing one cell group.
522 However, the nerve elements revealed by the markers had a specific arrangement in each type
523 of podia and formed a distinct nerve plate rich in cells and fibres.

524 Based on ultrastructural studies which identified numerous ciliated cells within the disc,
525 this structure is generally reported as the sensory part of the podia (Bouland et al., 1982;
526 Flammang & Jangoux, 1992; VandenSpiegel et al., 1995). In *H. arguinensis*, cell bodies
527 immunopositive to serotonin and NOS were found in the disc of the podia, some close to the
528 nerve plate and others between the epidermal cells (Figs. 11C-E). Whether these cells
529 correspond to the sensory neurons, as found in previous studies, remains to be determined. In
530 all cases, it is notable that fewer cells were stained with our markers in comparison with the
531 density of cell nuclei seen in the disc. This was also noted by Díaz-Balzac, Abreu-Arbelo, et al.
532 (2010) in the tentacles and tube feet of *H. glaberrima* using an antibody prepared against radial
533 nerve extracts from this species (called RN1). Further studies are thus needed to characterize
534 these cells.

Although it was not possible to carry out co-localization studies with the antibodies used in our study, staining of alternating serial sections with the different antibodies suggested that anti-NOS and anti-serotonin labelled different subpopulations of cells. Serotonin is an abundant neurotransmitter in the larval nervous system in echinoderms (e.g. Nakajima, Kaneko, Murray, & Burke, 2004; Nakano et al., 2006) but is poorly studied in adults (Beer, Moss, & Thorndyke, 2001). Its presence in adult echinoderm is still controversial and it is considered to be absent or very low abundance (Díaz-Balzac & García-Arrarás, 2018), which is in line with the relatively scarce serotonin immunopositive signal detected in the present study.

Interestingly, no glomeruli-like structures were found in *H. arguinensis;* this contrasts with the papillae and tentacles of the sea cucumber *Leptosynapta clarki* (Hoekstra et al., 2012). A possible explanation for the difference might be linked to the distinguishing characteristics of the order Apodida (to which *L. clarki* belongs) compared to the order Aspidochirotida (to which *H. arguinensis* belongs). Apodid holothuroids lack tube feet, retractor muscles in the pharynx, respiratory trees, and possess pinnate tentacles instead of the peltate tentacles seen in Aspidochirotida species (Ruppert & Barnes, 1994). However, we cannot exclude the possibility that the failure to detect glomeruli-like structures in *H. arguinensis* was due to technical issues and further studies will be required to clarify these results.

**4.4.Stem innervation**

The stems of the three types of podia presented the same nerve arrangement and had immunopositive cells and fibres with the three markers used. A few immunoreactive cells were seen in the stem of the podia, which agrees with previous ultrastructural (Cavey, 2006; Flammang & Jangoux, 1992) and immunohistochemical studies (Díaz-Balzac, Abreu-Arbelo, et al., 2010; Inoue et al., 1999). However, nitrergic fibres were particularly abundant in the podial nerve compared to those labelled with the other antibodies, and they may have a role in the stem mobility as explained in Section 4.2. Similarly, the fibres and cells labelled with anti-

serotonin in the same area could be involved in the regulation of muscle contraction, as demonstrated in pharmacological studies of the sea cucumber *Apostichopus japonicus* (Inoue et al., 2002). However, in general, the nerve fibres in the connective tissue were poorly labelled with our markers, with the exception of the anti-β-tubulin, suggesting a minor role for NO and serotonin in the connective nerve plexus previously described with the RN1 antibody (Díaz-Balzac et al., 2007). In the mesothelium, immunoreactive nerve fibres stained by our markers (NOS, serotonin, tubulin) and Palmgren's staining were clearly seen, and extended into, or came from, the stem nerve plexus, which is consistent with that found in *H. glaberrima* (Díaz-Balzac, Abreu-Arbelo, et al., 2010). However, the innervation of the podial mesothelium is suggested to come from indirect innervation by nerve fibres of the podial nerve that stop at the basal lamina of the mesothelium (Bouland et al., 1982; Cavey, 2006; Flammang & Jangoux, 1992). Therefore, further investigation is needed to understand the innervation of the mesothelium.

### 4.5.Concluding remarks

The present study revealed an abundance of NOS in the nervous system of the holothurian podia, which suggests NO has an important role as a neuronal messenger in these structures. The importance of NOS in the sea cucumber opens-up new research lines directed at determining its biological function. Our results confirmed that the disc of the podia is the most specialized area with a specific nervous arrangement, composed of a distinct nerve plate, rich in NOS, and containing numerous cells, some of which were anti-serotonin and anti-NOS positive. This structure seems to be a promising chemosensory candidate and a prime target for future electrophysiological assays. The tentacle disc might be interesting in relation to reproduction as it is always extended outside the oral cavity when the sea cucumber adopts its pre-spawning posture. However, it is unclear if this is a consequence of the hydrostatic pressure caused by the erect posture of the animal or a mechanism to improve chemical detection. If

electrophysiological experiments targeting the disc fail, the radial nerve cords could be an alternative, as have previously been used in starfish and brittle star (e.g. Binyon & Hasler, 1970; Brehm, 1977)

## Acknowledgements

This study was funded by national funds from FCT - Foundation for Science and Technology through project UIDB/04326/2020 and fellowship SFRH/BD/90761/2012 to NM. The authors thank Nadia Silva and Marco Campinho for their cooperation and advice on histological and immunohistochemical techniques. We also thank the Scigrades company (http://www.scigrades.be) for the sea cucumber diagram (figure 1) and João Afonso who helped to collect the animals.

## References


Beck, G., Ellis, T., Zhang, H., Lin, W., Beauregard, K., Habicht, G. S., & Truong, N. (2001). Nitric oxide production by coelomocytes of *Asterias forbesi*. *Developmental & Comparative Immunology, 25*(1), 1-10. doi:10.1016/S0145-305X(00)00036-7

Beer, A. J., Moss, C., & Thorndyke, M. (2001). Development of serotonin-like and SALMFamide-like immunoreactivity in the nervous system of the sea urchin *Psammechinus miliaris*. *The Biological Bulletin, 200*(3), 268-280. doi:10.2307/1543509

Binyon, J., & Hasler, B. (1970). Electrophysiology of the starfish radial nerve cord. *Comparative Biochemistry and Physiology, 32*(4), 747-753. doi:10.1016/0010-406X(70)90825-X

Bishop, C. D., & Brandhorst, B. P. (2007). Development of nitric oxide synthase-defined neurons in the sea urchin larval ciliary band and evidence for a chemosensory function during metamorphosis. *Developmental dynamics : an official publication of the American Association of Anatomists, 236*(6), 1535-1546. doi:10.1002/dvdy.21161

Bouland, C., Massin, C., & Jangoux, M. (1982). The fine structure of the buccal tentacles of *Holothuria forskali* (Echinodermata, Holothuroidea). *Zoomorphology, 101*(2), 133-149. doi:10.1007/bf00312019

Breer, H., & Shepherd, G. M. (1993). Implications of the NO/cGMP system for olfaction. *Trends Neurosci, 16*(1), 5-9. doi:10.1016/0166-2236(93)90040-s

Brehm, P. (1977). Electrophysiology and luminescence of an ophiuroid radial nerve. *The Journal of experimental biology, 71*, 213-227.

Bruning, G. (1994). NADPH diaphorase histochemistry in the adrenal gland of the mouse. *Acta Histochemica, 96*(2), 205-211. doi:10.1016/s0065-1281(11)80179-0

Caballes, C. F., & Pratchett, M. S. (2017). Environmental and biological cues for spawning in the crown-of-thorns starfish. *PLoS ONE, 12*(3), e0173964. doi:10.1371/journal.pone.0173964

Campbell, A. C., Coppard, S., D'Abreo, C., & Tudor-Thomas, R. (2001). Escape and aggregation responses of three echinoderms to conspecific stimuli. *The Biological Bulletin, 201*, 175-185. doi:10.2307/1543332

Cavey, M. J. (2006). Organization of the coelomic lining and a juxtaposed nerve plexus in the suckered tube feet of *Parastichopus californicus* (Echinodermata: Holothuroida). *Journal of Morphology, 267*(1), 41-49. doi:10.1002/jmor.10386

Cobb, J. L. (1978). An ultrastructural study of the dermal papulae of the starfish, *Asterias rubens*, with special reference to innervation of the muscles. *Cell and Tissue Research, 187*(3), 515-523. doi:10.1007/BF00229616

Cobb, J. L. S. (1987). Neurobiology of the Echinodermata. In M. A. Ali (Ed.), *Nervous systems in invertebrates* (pp. 483-525). Boston, MA: Springer US.

Colasanti, M., & Venturini, G. (1998). Nitric oxide in invertebrates. *Mol Neurobiol, 17*(1-3), 157-174. doi:10.1007/bf02802029

Cooke, I. R. C., Edwards, S. L., & Anderson, C. R. (1994). The distribution of NADPH diaphorase activity and immunoreactivity to nitric oxide synthase in the nervous system of the pulmonate mollusc *Helix aspersa*. *Cell and Tissue Research, 277*(3), 565-572. doi:10.1007/BF00300230

Cyrus, M. D., Bolton, J. J., Scholtz, R., & Macey, B. M. (2015). The advantages of Ulva (Chlorophyta) as an additive in sea urchin formulated feeds: effects on palatability, consumption and digestibility. *Aquaculture Nutrition, 21*(5), 578-591. doi:10.1111/anu.12182

Dawson, T. M., Bredt, D. S., Fotuhi, M., Hwang, P. M., & Snyder, S. H. (1991). Nitric oxide synthase and neuronal NADPH diaphorase are identical in brain and peripheral tissues. *Proceedings of the National Academy of Sciences of the United States of America, 88*(17), 7797-7801. doi:10.1073/pnas.88.17.7797

Díaz-Balzac, C. A., Abreu-Arbelo, J. E., & García-Arrarás, J. E. (2010). Neuroanatomy of the tube feet and tentacles in *Holothuria glaberrima* (Holothuroidea, Echinodermata). *Zoomorphology, 129*(1), 33-43. doi:10.1007/s00435-009-0098-4

Díaz-Balzac, C. A., & García-Arrarás, J. (2018). Echinoderm Nervous System. *Oxford Research Encyclopedia of Neuroscience*, 1-31. doi:10.1093/acrefore/9780190264086.013.205

Díaz-Balzac, C. A., Lazaro-Pena, M. I., Vazquez-Figueroa, L. D., Diaz-Balzac, R. J., & Garcia-Arraras, J. E. (2016). Holothurian nervous system diversity revealed by neuroanatomical analysis. *PLoS ONE, 11*(3), e0151129. doi:10.1371/journal.pone.0151129

Díaz-Balzac, C. A., Mejías, W., Jiménez, L. B., & García-Arrarás, J. E. (2010). The catecholaminergic nerve plexus of Holothuroidea. *Zoomorphology, 129*(2), 99-109. doi:10.1007/s00435-010-0103-y

Díaz-Balzac, C. A., Santacana-Laffitte, G., San Miguel-Ruiz, J. E., Tossas, K., Valentin-Tirado, G., Rives-Sanchez, M., . . . Garcia-Arraras, J. E. (2007). Identification of nerve plexi in connective tissues of the sea cucumber *Holothuria glaberrima* by using a novel nerve-specific antibody. *The Biological Bulletin, 213*(1), 28-42. doi:10.2307/25066616

Díaz-Balzac, C. A., Vázquez-Figueroa, L. D., & García-Arrarás, J. E. (2014). Novel markers identify nervous system components of the holothurian nervous system. *Invertebrate Neuroscience, 14*(2), 113-125. doi:10.1007/s10158-014-0169-1

Díaz-Miranda, L., Blanco, R. E., & Garcia-Arraras, J. E. (1995). Localization of the heptapeptide GFSKLYFamide in the sea cucumber *Holothuria glaberrima* (Echinodermata): a light and electron microscopic study. *The Journal of comparative neurology, 352*(4), 626-640. doi:10.1002/cne.903520410

Dix, T. G. (1969). *The biology of the echinoid Evechinus chloroticus (val.) in different habitats.* (PhD Dissertation), University of Canterbury, New Zealand,

Elofsson, R., Carlberg, M., Moroz, L., Nezlin, L., & Sakharov, D. (1993). Is nitric oxide (NO) produced by invertebrate neurones? *Neuroreport, 4*(3), 279-282. doi:10.1097/00001756-199303000-00013

Elphick, M. R. (1997). Localization of nitric oxide synthase using NADPH-diaphorase histochemistry. In R. C. Rayne (Ed.), *Neurotransmitter methods* (pp. 153-158). Totowa, NJ: Springer New York.

Elphick, M. R., Green, I. C., & O'Shea, M. (1994). Nitric oxide signalling in the insect nervous system. In A. B. Borkovec & M. Loeb (Eds.), *Insect neurochemistry and neurophysiology* (pp. 129-132.). Boca Raton: CRC Press.

Elphick, M. R., & Melarange, R. (1998). Nitric oxide function in an echinoderm. *The Biological Bulletin, 194*(3), 260-266. doi:10.2307/1543096

Flammang, P. (1996). Adhesion in Echinoderms. In M. Jangoux & J. M. Lawrence (Eds.), *Echinoderm Studies* (Vol. 5, pp. 1-60). Rotterdam: Balkema.

Flammang, P., & Jangoux, M. (1992). Functional morphology of the locomotory podia of *Holothuria forskali* (Echinodermata, Holothuroida). *Zoomorphology, 111*(3), 167-178. doi:10.1007/bf01632906

Flammang, P., Ridder, C., & Jangoux, M. (1991). Ultrastructure of the pencillate podia of the spatangoid echinoid *Echinocardium cordatum* (Echinodermata) with special emphasis on the epidermal sensory-secretory complex. *Acta Zoologica, 72*, 151-158. doi:10.1111/j.1463-6395.1991.tb00942.x

Florey, E., & Cahill, M. A. (1977). Ultrastructure of sea urchin tube feet. *Cell and Tissue Research, 177*(2), 195-214. doi:10.1007/bf00221081

Gelperin, A. (1994). Nitric oxide mediates network oscillations of olfactory interneurons in a terrestrial mollusc. *Nature, 369*(6475), 61-63. doi:10.1038/369061a0

Gillette, R. (2006). Evolution and Function in Serotonergic Systems. *Integrative and Comparative Biology, 46*(6), 838-846. doi:10.1093/icb/icl024

Hamel, J.-F., & Mercier, A. (1996). Evidence of chemical communication during the gametogenesis of holothurids. *Ecology, 77*(5), 1600-1616.

Hoekstra, L. A., Moroz, L. L., & Heyland, A. (2012). Novel insights into the echinoderm nervous system from histaminergic and FMRFaminergic-like cells in the sea cucumber *Leptosynapta clarki*. *PLoS ONE, 7*(9), e44220. doi:10.1371/journal.pone.0044220

Holland, N. D. (1984). Epidermal cells. In J. Bereiter-Hahn, A. G. Matoltsy, & K. S. Richards (Eds.), *Biology of the integument: invertebrates* (pp. 756-774). Berlin, Heidelberg: Springer Berlin Heidelberg.

Holmqvist, B. I., Ostholm, T., Alm, P., & Ekstrom, P. (1994). Nitric oxide synthase in the brain of a teleost. *Neuroscience Letters, 171*(1-2), 205-208. doi:10.1016/0304-3940(94)90640-8

Hope, B. T., Michael, G. J., Knigge, K. M., & Vincent, S. R. (1991). Neuronal NADPH-diaphorase is a nitric oxide synthase. *Proceedings of the National Academy of Sciences of the United States of America, 88*(7), 2811-2814. doi:10.1073/pnas.88.7.2811

Humason, G. L. (1972). *Animal tissue techniques*. San Francisco: W.H. Freeman.

Hyman, L. H. (1955). *The Invertebrates, Vol. 4, Echinodermata*. New-York, USA.

Inoue, M., Birenheide, R., Koizumi, O., Kobayakawa, Y., Muneoka, Y., & Motokawa, T. (1999). Localization of the neuropeptide NGIWYamide in the holothurian nervous system and its effects on muscular contraction. *Proceedings of the Royal Society B: Biological Sciences, 266*(1423), 993-993. doi:10.1098/rspb.1999.0735

Inoue, M., Tamori, M., & Motokawa, T. (2002). Innervation of holothurian body wall muscle: inhibitory effects and localization of 5-HT. *Zoolog Sci, 19*(11), 1217-1222. doi:10.2108/zsj.19.1217

Jacklet, J. W. (1997). Nitric oxide signaling in invertebrates. *Invertebrate Neuroscience, 3*(1), 1-14. doi:10.1007/bf02481710

Johansson, K. U. I., & Carlberg, M. (1995). NO-synthase: What can research on invertebrates add to what is already known? *Advances in Neuroimmunology, 5*(4), 431-442. doi:10.1016/0960-5428(95)00027-5

Leckie, C., Empson, R., Becchetti, A., Thomas, J., Galione, A., & Whitaker, M. (2003). The NO pathway acts late during the fertilization response in sea urchin eggs. *Journal of Biological Chemistry, 278*(14), 12247-12254. doi:10.1074/jbc.M210770200

Mann, K. H., Wright, J. L. C., Welsford, B. E., & Hatfield, E. (1984). Responses of the sea urchin *Strongylocentrotus droebachiensis* (O.F. Müller) to water-borne stimuli from potential predators and potential food algae. *Journal of Experimental Marine Biology and Ecology, 79*(3), 233-244. doi:10.1016/0022-0981(84)90197-7

Marquet, N., Hubbard, P. C., da Silva, J. P., Afonso, J., & Canário, A. V. M. (2018). Chemicals released by male sea cucumber mediate aggregation and spawning behaviours. *Scientific Reports, 8*(1), 239. doi:10.1038/s41598-017-18655-6

Martínez, A. (1995). Nitric oxide synthase in invertebrates. *The Histochemical Journal, 27*(10), 770-776. doi:10.1007/bf02388302

Martínez, A., Riveros-Moreno, V., Polak, J. M., Moncada, S., & Sesma, P. (1994). Nitric oxide (NO) synthase immunoreactivity in the starfish *Marthasterias glacialis*. *Cell and Tissue Research, 275*(3), 599-603. doi:10.1007/bf00318828

McKenzie, J. D. (1987). The ultrastructure of the tentacles of eleven species of dendrochirote holothurians studied with special reference to the surface coats and papillae. *Cell and Tissue Research, 248*(1), 187-199. doi:10.1007/bf01239980

Meulemans, A., Mothet, J. P., Schirar, A., Fossier, P., Tauc, L., & Baux, G. (1995). A nitric oxide synthase activity is involved in the modulation of acetylcholine release in Aplysia ganglion neurons: a histological, voltammetric and electrophysiological study. *Neuroscience, 69*(3), 985-995. doi:10.1016/0306-4522(95)00316-b

Moncada, S., Palmer, R. M., & Higgs, E. A. (1991). Nitric oxide: physiology, pathophysiology, and pharmacology. *Pharmacological Reviews, 43*(2), 109-142.

Moore, S. J., & Thorndyke, M. C. (1993). Immunocytochemical mapping of the novel echinoderm neuropeptide SALMFamide 1 (S1) in the starfish *Asterias rubens*. *Cell and Tissue Research, 274*(3), 605-618. doi:10.1007/bf00314559

Moroz, L. L. (2006). Localization of putative nitrergic neurons in peripheral chemosensory areas and the central nervous system of *Aplysia californica*. *Journal of Comparative Neurology, 495*. doi:10.1002/cne.20842

Moroz, L. L., Meech, R. W., Sweedler, J. V., & Mackie, G. O. (2004). Nitric oxide regulates swimming in the jellyfish *Aglantha digitale*. *The Journal of comparative neurology, 471*(1), 26-36. doi:10.1002/cne.20023

Moroz, L. L., Winlow, W., Turner, R. W., Bulloch, A. G., Lukowiak, K., & Syed, N. I. (1994). Nitric oxide synthase-immunoreactive cells in the CNS and periphery of Lymnaea. *Neuroreport, 5*(10), 1277-1280. doi:10.1097/00001756-199406020-00031

Müller, U. L. I. (1997). The nitric oxide system in insects. *Progress in Neurobiology, 51*(3), 363-381. doi:10.1016/S0301-0082(96)00067-6

Nacsa, K., Elekes, K., & Serfőző, Z. (2015). Ultrastructural localization of NADPH diaphorase and nitric oxidesynthase in the neuropils of the snail CNS. *Micron, 75*, 58-66. doi:10.1016/j.micron.2015.04.015

Nakajima, Y., Kaneko, H., Murray, G., & Burke, R. D. (2004). Divergent patterns of neural development in larval echinoids and asteroids. *Evol Dev, 6*(2), 95-104.

Nakano, H., Murabe, N., Amemiya, S., & Nakajima, Y. (2006). Nervous system development of the sea cucumber *Stichopus japonicus*. *Dev Biol, 292*(1), 205-212. doi:10.1016/j.ydbio.2005.12.038

Palumbo, A. (2005). Nitric oxide in marine invertebrates: a comparative perspective. *Comparative Biochemistry and Physiology Part A: Molecular & Integrative Physiology, 142*(2), 241-248. doi:10.1016/j.cbpb.2005.05.043

Pentreath, V. W., & Cobb, J. L. S. (1972). Neurobiology of Echinodermata *Biological Reviews, 47*(3), 363-392. doi:10.1111/j.1469-185X.1972.tb00977.x

Ruppert, E. E., & Barnes, R. D. (1994). *Invertebrate Zoology*. Orlando, Florida: Saunders College Publishing, Harcourt Brace and Company.

Santos, R., Haesaerts, D., Jangoux, M., & Flammang, P. (2005). Comparative histological and immunohistochemical study of sea star tube feet (Echinodermata, Asteroidea). *Journal of Morphology, 263*(3), 259-269. doi:10.1002/jmor.10187

Snyder, S. H., & Bredt, D. S. (1991). Nitric oxide as a neuronal messenger. *Trends in Pharmacological Sciences, 12*, 125-128. doi:10.1016/0165-6147(91)90526-X

Soong, K., Chang, D., & Chao, S. M. (2005). Presence of spawn-inducing pheromones in two brittle stars (Echinodermata: Ophiuroidea). *Marine Ecology Progress Series, 292*, 195-201. doi:10.3354/meps292195

Talavera, E., Martfnez-Lorenzana, G., León-Olea, M., Sánchez-Alvarez, M., Sánchez-Islas, E., & Pellicer, F. (1995). Histochemical distribution of NADPH-diaphorase in the cerebral ganglion of the crayfish *Cambarellus montezumae*. *Neuroscience Letters, 187*(3), 177-180. doi:10.1016/0304-3940(95)11368-7

Tamori, M., Saha, A. K., Matsuno, A., Noskor, S. C., Koizumi, O., Kobayakawa, Y., . . . Motokawa, T. (2007). Stichopin-containing nerves and secretory cells specific to connective tissues of the sea cucumber. *Proceedings. Biological sciences, 274*(1623), 2279-2285. doi:10.1098/rspb.2007.0583

Ullrich-Lüter, E. M., Dupont, S., Arboleda, E., Hausen, H., & Arnone, M. I. (2011). Unique system of photoreceptors in sea urchin tube feet. *Proceedings of the National Academy of Sciences, 108*(20), 8367. doi:10.1073/pnas.1018495108

Unger, B., & Lott, C. (1994). In-situ studies on the aggregation behaviour of the sea urchin *Sphaerechinus granularis* Lam. (Echinodermata: Echinoidea). In B. David, A. Guille, J. P. Feral, & M. Roux (Eds.), *Echinoderms through time.* (pp. 919-919). Rotterdam: AA Balkema.

VandenSpiegel, D., Flammang, P., Fourmeau, D., & Jangoux, M. (1995). Fine structure of the dorsal papillae in the holothurioid *Holothuria forskali* (Echinodermata). *Tissue & cell, 27*(4), 457-465. doi:10.1016/S0040-8166(95)80066-2

Villar, M. J., Settembrini, B. P., Hokfelt, T., & Tramezzani, J. H. (1994). NOS is present in the brain of *Triatoma infestans* and is colocalized with CCK. *Neuroreport, 6*(1), 81-84. doi:10.1097/00001756-199412300-00022

**Supporting information**

**Figure S1.** Histology, NADPH-histochemistry and NOS immunohistochemistry of the body wall including the radial nerve cord (RNC). **A** Transverse section through the body wall stained with Masson's Trichrome showing the loose (*lct*) and dense (*dct*) connective tissue *in green*, the radial nerve cord (*rnc*) in *dark pink*, the circular (*cm*) and longitudinal (*lm*) muscles in *red*. **B** Surface part of the body wall showing the distribution of the ossicles and (insert) typical ossicles (*os*) stained with Alizarin red. **C** Deeper part of the body wall highlighting the radial nerve cord stained with Milligan's Trichrome. **D – E** Positive histochemical reaction for NADPH-d in the RNC (D) and absence of reactivity in the control (E). **F – G** Immunopositivity to anti-NOS (F) in the RNC and the absence of signal in the control (G). *cu*: cuticle, *cl*: connective tissue layer, *es*: epineural sinus, *en*: ectoneural neuroepithelium, *ep*: epidermis, *h*: haemal lacuna, *hs*: hyponeural sinus, *hn*: hyponeural neuroepithelium, *rnc:* radial nerve cord, *wvs*: water vascular canal. D, P (in all panels) indicate distal and proximal orientations. Scale bars: 100 µm.

**Figure S2.** Immunohistochemistry of the radial nerve cord. **A** Serotonin immunolabeling is mainly distributed in the central and lateral region of the ectoneural (*en*) part of the RNC and in the central region of the hyponeural (*hn*) part of the RNC. **B** An extensive positive reaction to anti-NOS is present in both parts of the RNC. **C** Control slide where only the secondary anti-rabbit antibody was applied. **D** DAPI-stained section showing the abundance of cell nuclei lining the ectoneural (arrow) and hyponeural (arrowhead) components of the RNC, and the region with relatively lower abundance of cell nuclei within the RCN. **E** Tubulin immunoreactivity is largely distributed in both parts of the RNC. **F** Control slide where only the secondary anti-mouse antibody was applied. D, P (in all panels) indicate distal and proximal orientations. Scale bars: 100 µm.

**Figure S3.** Treatment (NADPH-d and anti-NOS) (A, C) and control (B, D) slides in the stem of the tentacle. **A – B** Reactivity to NADPH-d in the treatment section (A) and absence of reactivity in the control (B). **C – D** Immunopositivity to anti-NOS in the treatment section (C) and control where anti-NOS was omitted (D). C, M (in all panels) indicate central and marginal orientations Scale bars: 100 µm.

**Figure S4.** Treatment (NADPH-d and anti-NOS) (A, C) and control (B, D) slides in a bud of the tentacle. **A – B.** Reactivity to NADPH-d in the treatment section (A) and absence of reactivity in the control (B). **C – D.** Immunopositivity to anti-NOS in the treatment section (C) and control where anti-NOS was omitted (D). P, D (in all panels) indicate proximal and distal orientations. Scale bars: 100 µm.

**Figure S5.** Treatment (B, C, E) and control (A, D) slides in the disc of the tentacle. **A** Control slide where only the secondary anti-rabbit antibody was applied and **B – C** the treatment slides using the same secondary antibody with (B) anti-NOS and (C) anti-serotonin. **D** Control slide where anti-tubulin was omitted and only the secondary anti-mouse antibody was applied and **E** a section with the anti-tubulin primary antibody and the anti-mouse secondary antibody. P, D (in all panels) indicate proximal and distal orientations. Scale bars: 25µm.

**Figure S6.** Treatment (NADPH-d and anti-NOS) (A, C) and control (B, D) slides in the tube feet. **A – B** Reactivity to NADPH-d in the treatment slide (A) and absence of reactivity in the control slide (B). **C – D** Immunoreactivity to anti-NOS in the treatment slide (C) and control slide where anti-NOS was omitted (D). P, D (in all panels) indicate proximal and distal orientations. Scale bars: 100 µm.

**Figure S7.** Treatment (B, C, E) and control (A, D) slides in the disc of the tube feet. **A** Control section where only the secondary anti-rabbit antibody was applied, and **B** anti-NOS and **C** anti-serotonin primary antisera was used with the anti-rabbit secondary antibody. **D** Control where only the secondary anti-mouse antibody was applied and **E** the treatment section using anti-

tubulin and anti-mouse secondary antibody. P, D (in all panels) indicate proximal and distal orientations. Scale bars: 25µm.

**Figure S8.** Treatment (B, C, E) and control (A, D) sections in the stem of the body wall. **A** Control section where only the secondary anti-rabbit antibody was applied and **B** anti-NOS and **C** anti-serotonin primary antisera with the anti-rabbit secondary antibody. **D** Control sections where only the secondary anti-mouse antibody was applied and **E** the treatment sections using anti-tubulin and anti-mouse secondary antibody. C, M (in all panels) indicate central and marginal orientations. Scale bars: 25µm.

**Figure S9.** Treatment (NADPH-d and anti-NOS) (A, C) and control (B, D) in the pointed structure of the papillae. **A** Reactivity to NADPH-d in the treatment section and **B** absence of reactivity in the control. **C** Immunoreactivity to anti-NOS in the treatment section and **D** control. P, D (in all panels) indicate proximal and distal orientations. Scale bars: 50 µm in A, B and 100 µm in C, D.

**Figure S10.** Treatment (NADPH-d and anti-NOS) (A, C) and control (B, D) in the stem of the papillae. **A** Reactivity to NADPH-d in the treatment section and **B** absence of reactivity in the control. **C** Immunoreactivity to anti-NOS in the treatment section and **D** control. P, D (in all panels) and C, M (in C, D) indicate respectively, proximal, distal, central and marginal orientations. Scale bars: 100 µm.

**Figure S11.** Treatment (A, C, D, F) and control (B, E) in the pointed structure of the papillae. **A** Section stained with DAPI in which the white rectangle delineates the area of the papillae shown in each treatment section. **B** Control where only the secondary anti-rabbit antibody was applied and the treatment slides **C** anti-NOS and **D** anti-serotonin using the anti-rabbit secondary antibody. **E** Control where only the secondary anti-mouse antibody was applied and the treatment section **F** with anti-tubulin and anti-mouse secondary antibody. P, D (in all panels) indicate proximal and distal orientations. Scale bars: 25µm.

**Figures legends**

**Figure 1.** Schematic representation of *H. arguinensis* revealing the salient external morphological features. **A** General view of *H. arguinensis*. **B** Enlargement of the oral cavity highlighting the peltate tentacles. A: anterior, P: posterior, D: dorsal and V: ventral. Not to scale.

**Figure 2.** Histology of the tentacle. **A** Macroscopic photograph of the oral cavity showing the crown of tentacles (*t*) surrounding the mouth. **Insert** Each tentacle was composed of a stem (*st*) and a distal disc (*d*). **B-D** Longitudinal section through the tentacle stained with Masson's trichrome (B-C) showing the external (*ect*), central (*cct*) and inner (*ict*) connective tissue in *green*, the mesothelium (*me*) in *red*, and the buccal nerve (*bn*) in *light red*; and stained with Palmgren's stain (D) showing the buccal nerve (*bn*) in *dark brown* and the ossicles (*os*) in *black*. **E - F** Higher magnification (E) of the centre of the stem where nerves stained in *black* are seen in the mesothelium (arrows) and, (F) in the bud where apical neurites (arrows) project from the nerve plate (arrowhead) into the epidermis. **G** Transverse section of the tentacle stem stained with Miligan's Trichrome showing the longitudinal buccal nerve (*lbn*) and the buccal nerve plexus (*bn*) in *light purple,* the mesothelium (*me*) in *magenta* and the connective tissue (*ict*: internal connective tissue, *cct*: central connective tissue) in *blue. al*: ambulacral lumen, *bu*: bud, *cu*: cuticle, *pa*: papilla. D, P (in A, B, C, E, F) and C, M (in G) indicate respectively, distal, proximal, central and marginal orientations. Scale bars: 100 µm.

**Figure 3.** NADPH-d histochemistry and NOS immunohistochemistry of the tentacle. **A-B** Transverse section of the stem of the tentacle showing a strong positive histochemical reaction for NADPH-d (A) and immunoreactivity with anti-NOS antibodies (B) in the buccal nerve (*bn*) and the longitudinal buccal nerve (*lbn*), and a less intense signal for both markers in the mesothelium (*me*). **C – F** Higher power magnification of the longitudinal buccal nerve (C-D) and, the buccal nerve and mesothelium (E-F) showing anti-NOS (C, E) and NADPH-d (D, F)

reactivity. **G - H** The papilla of a tentacle where NADPH-d reactivity (G) and anti-NOS immunoreactivity (H) were strong in the buccal nerve and less intense in the mesothelium, and where fibres reactive with both markers (NADPH-d and anti-NOS, arrows) were seen in the epidermis (*ep*) of the two buds. **I - K** Higher magnification of the epidermis of a tentacle bud showing fibres (arrows) immunoreactive with anti-NOS (I, K) and NADPH-d (J) in the extremity of the bud as well as in the nerve plate (*np*), with some cell-bodies reactive with both markers (arrowheads). *cct*: central connective tissue. C, M (in A, B, C, D, E, F) and P, D (in G, H, I, J, K) indicate respectively, central, marginal, proximal and distal orientations. Scale bars: 100 µm in A– H, 25 µm in I – J and 5 µm in K.

**Figure 4.** Comparison of anti-NOS, anti-serotonin and anti-tubulin immunoreactivity in the tentacle disc. **A** Nitrergic fibres found in the upper area in contact with the environment (arrowhead), in the buccal nerve (*bn*; horizontal arrow) and in the nerve plate (*np*; vertical arrows). **B** Serotonin positive cell bodies (arrowhead; insert) in the epidermal cells and immunoreactive fibres were also identified in the nerve plate (vertical arrow) and the buccal nerve (horizontal arrows). **C** Tubulin positive immunofluorescence in the buccal nerve plexus (horizontal arrow), in some fibres in the nerve plate (vertical arrow) and within the cell clusters (arrowhead). **D** DAPI-stained section showing the distribution of cells within the bud. *ep*: epidermis. D and P in all panels indicate distal and proximal orientations. Scale bars: 25 µm and in all inserts: 5 µm.

**Figure 5.** Histology of the tube feet. **A** Macroscopic photograph of the podia showing the stem (*st*) and the distal disc (*d*) from the ventral side. **B** Longitudinal section of the podia stained with Milligan's Trichrome showing the tissue layer subdivision: cuticle (*cu*), epidermis (*ep*), connective tissue (*ct*) in *blue* (external connective tissue, *ect*; central connective tissue, *cct;* internal connective tissue, *ict*), longitudinal podial nerve (*lpn*) and podial nerve plexus (arrowheads) in *light purple*, and mesothelium (*me*) in *magenta*. **C** Higher magnification of the

terminal disc on the tube feet showing the inner (*icc*) and outer (*occ*) clusters of cells, surrounded by the connective tissue above the occ (arrows) and between them (arrowheads). **D - E** Higher magnification of the longitudinal podial nerve stained with Milligan's Trichrome (D) and of the upper part of the tube feet stained with Palmgren's (E) showing the heavily stained nerve fibres (red arrowheads). The white rectangle indicates the black deposits corresponding to the calcified ossicles. **F** Alizarin red staining showing the ossicles (*os*) and the supporting ossicles (*so*). D, P (in A, B, C, E, F) and C, M (in D) indicate respectively, distal, proximal, central and marginal orientations. Scale bars: 100 µm.

**Figure 6.** NADPH-d histochemistry and NOS immunohistochemistry of the tube feet. **A – B** Positive histochemical reaction to NADPH-d (A) and immunoreactivity to anti-NOS (B) in the stem highlighting the podial nerve plexus (*pn*) extending into the mesothelium (*me*) and connective tissue (*ct*) and in the nerve plate of the distal disc (arrows). **C – E** Higher magnification of the stem showing fibres (arrows) reactive with NADPH-d (C) and anti-NOS (D) in the podial nerve, and in the mesothelium (E). **F – H** Higher magnification of the distal disc showing fibres reactive to NADPH-d (F) and anti-NOS (G) in the nerve plate (arrows), and highlighting the presence of cell bodies immunoreactive with anti-NOS in the cell clusters of the disc (arrowhead) (H). D, P (in A, B, C, D, E, F, G, H) and C, M (in A, B, C, D, E) indicate respectively, distal, proximal, central and marginal orientations. Scale bars: A – E and G:100 µm and F, H: 20 µm.

**Figure 7.** Comparison of anti-NOS, anti-serotonin and anti-tubulin immunoreactivity in the tube feet disc and stem. **A – D** Tube feet disc. **A** Nitrergic fibres coming from the nerve plate are seen in both cell clusters (horizontal arrows; outer cluster of cell, *occ*; inner cluster of cells, *icc*) and a few cell bodies immunopositive with anti-NOS (arrowhead; insert) could be found in proximity to the nerve plate (*np*). **B** Serotonin immunoreactivity is present in fibres projecting from the nerve plate and in cell clusters (arrows). A few serotonin immunoreactive cell bodies

are present around the nerve plate (arrowheads; insert). **C** Fibres immunopositive with anti-tubulin are present in the nerve plate (vertical arrow) and between the nerve plate and the two cell clusters (horizontal arrows). **D** DAPI-stained section showing the nuclei of the densely packed outer cell cluster and the loosely packed inner cell cluster. **E – H** Tube feet stem. The same general tissue organization was observed in the stem of the papillae and the tentacle. **E** An abundance of NOS-immunopositive nitrergic fibres are present in the podial nerve plexus (*pn*) (vertical arrow) compared to the connective tissue (*ct*) and the mesothelium (*me*) (horizontal arrows). Only a few nitrergic cell bodies were found in the podial nerve plexus (arrowhead; insert). **F** Serotonin-immunopositive cell bodies (arrowhead; insert) in the podial nerve plexus, and fibres (arrows) in both the podial nerve plexus and mesothelium. **G** Strong immunoreactivity to anti-tubulin in the podial nerve plexus, the mesothelium and connective tissue (fibres: arrows). **H** DAPI-stained section indicating the main structures: connective tissue (*ct*), podial nerve plexus (*pn*) and mesothelium (*me*). al: ambulacral lumen. D, P (in A, B, C, D) and C, M (in E, F, G, H) indicate respectively, distal, proximal, central and marginal orientations. Scale bars: 25 µm and in all inserts: 5 µm.

**Figure 8.** Histology of the papillae. **A** Macroscopic photograph of the dorsal side showing two papillae and (*insert*) a higher magnification of a papillae showing the stem (*st*) and the white distal disc (*d*). **B** Distribution of the ossicles (*os*) in the papillae. The boxed regions in A and B are shown in higher magnification in photographs C and E. **C** Higher magnification of the stem stained with Milligan's trichrome clearly showing the connective tissue (*ict:* internal and *cct:* central) in *blue*, the longitudinal papillae nerve (*lpan*) and papillae nerve plexus (arrowheads) in *light purple*, the mesothelium (*me*) in *magenta* and the ambulacral lumen (*al*); with (*inser*t) Palmgren's staining showing nervous fibres in the papillae nerve plexus (*pan*) in *black* (arrows). **D – E** Higher magnification of the distal disc stained with (D) H&E and (E) Palmgren's showing the nerve fibres (arrowheads) in *black.* D, P (in A, B, C, D, E) and C, M (in B, C)

indicate respectively, distal, proximal, central and marginal orientations. Scale bars: A: 500 µm, B, D, E: 100 µm and C in insert 25 µm.

**Figure 9.** NADPH-d histochemistry and NOS immunohistochemistry of the papillae. **A** Section under bright field light of the terminal part of the papillae showing the localization of the ossicles (arrow). **B – C** Positive NOS-immunoreactivity (B; asterisks localize the ossicles) and NADPH-d staining (C) in the terminal part of the papillae showing some nitrergic fibres (arrows) and cell bodies (arrowheads), with a higher magnification of a nitrergic cell body presented in the insert in B. **D** – **F** Stem of the papillae showing strong NOS-immunoreactivity (D, E) and NADPH-d (F) in the papillae nerve (*pan*), with a weaker signal in the mesothelium (*me*) (fibres: arrows and cell bodies: arrowheads). *al*: ambulacral lumen, *ct*: connective tissue. D, P (in all panels) and M, C (in D, E, F) indicate respectively, distal, proximal, marginal and central orientations. Scale bars: 100 µm in all figures; insert in B: 10 µm.

**Figure 10.** Comparison of anti-NOS, anti-serotonin and anti-tubulin immunoreactivity in the terminal end of a papillae. **A** Immunoreactive nitrergic fibres (arrows) and cell bodies (arrowhead; insert), and **B** immunoreactive serotonin cell bodies (arrowhead; insert) could be seen in the epidermal cells. **C** Tubulin immunofluorescence in fibres (arrows) and **D** DAPI-stained sections show the abundance of nuclei in the terminal disc of the papillae. D and P in all panels indicate distal and proximal orientations. Scale bars: 25 µm and all inserts: 5 µm.

**Figure 11.** Schematic diagrams of the holothurian podia. **A** Longitudinal representation of a podia's stem showing the disc (*d*) and the stem (*st*) containing the following layers: cuticle (*cu*) in *black*, epidermis (*ep*) in *grey*, connective tissue (*ct*) in *green*, podial nerve (*pn*) in *red* and mesothelium (*me*) in *orange*. D, P, M, and C indicate distal, proximal, marginal and central orientations, respectively. **B** Higher magnification of the stem tissue layers where the distribution of fibres and cell bodies labelled with anti-NOS (*black*) and anti-serotonin (*grey*) are schematically represented in the central connective tissue (*cct*), podial nerve (*pn*), internal

connective tissue (*ict*) and mesothelium (*me*). **C – E** Higher magnification of the three types of holothurian's disc where the distribution of fibres and cell bodies labelled with anti-NOS (*black*) and anti-serotonin (*grey*) are schematically represented in the tentacle (C), tube feet (D) and papillae (E). *ep*: epidermis, *icc*: inner cluster of cells, *np*: nerve plate, *occ*: outer cluster of cells, *os*: ossicles.

## Tables legends

**Table 1.** Antibodies used in this study, their origin and working conditions.

| **Antigen** | **Raised in** | **Immunogen** | **Source** | **Dilution** |
|---|---|---|---|---|
| NOS | Rabbit (polyclonal) | Synthetic peptide (Asp-Gln-Lys-Arg-Tyr-His-Glu-Asp-Ile-Phe-Gly), derived from amino acids 1113-1122 with N-terminally added Asp, of mouse iNOS and nNOS. | Sigma (N-217) | 1:100 |
| β-tubulin | Mouse (monoclonal) | Tubulin from rat brain, clone TUB 2.1, ascites fluid | Sigma (T-4026) | 1:250 |
| Serotonin | Rabbit (polyclonal) | Serotonin creatinine sulfate complex conjugated with formaldehyde to BSA | Sigma (S-5545) | 1:400 |

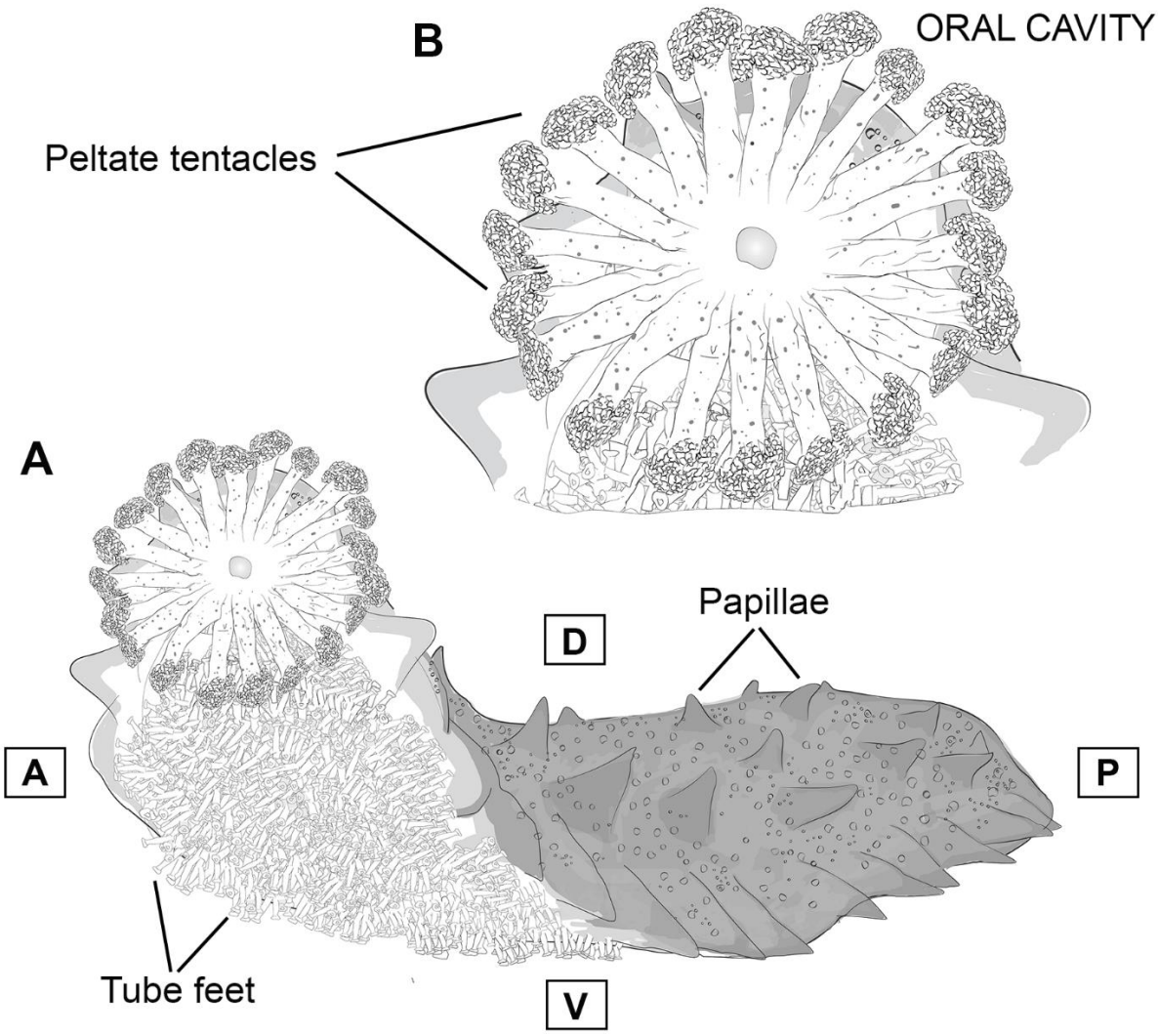


**Figure 1.** Schematic representation of *H. arguinensis* revealing the salient external morphological features. **A** General view of *H. arguinensis*. **B** Enlargement of the oral cavity highlighting the peltate tentacles. A: anterior, P: posterior, D: dorsal and V: ventral. Not to scale.

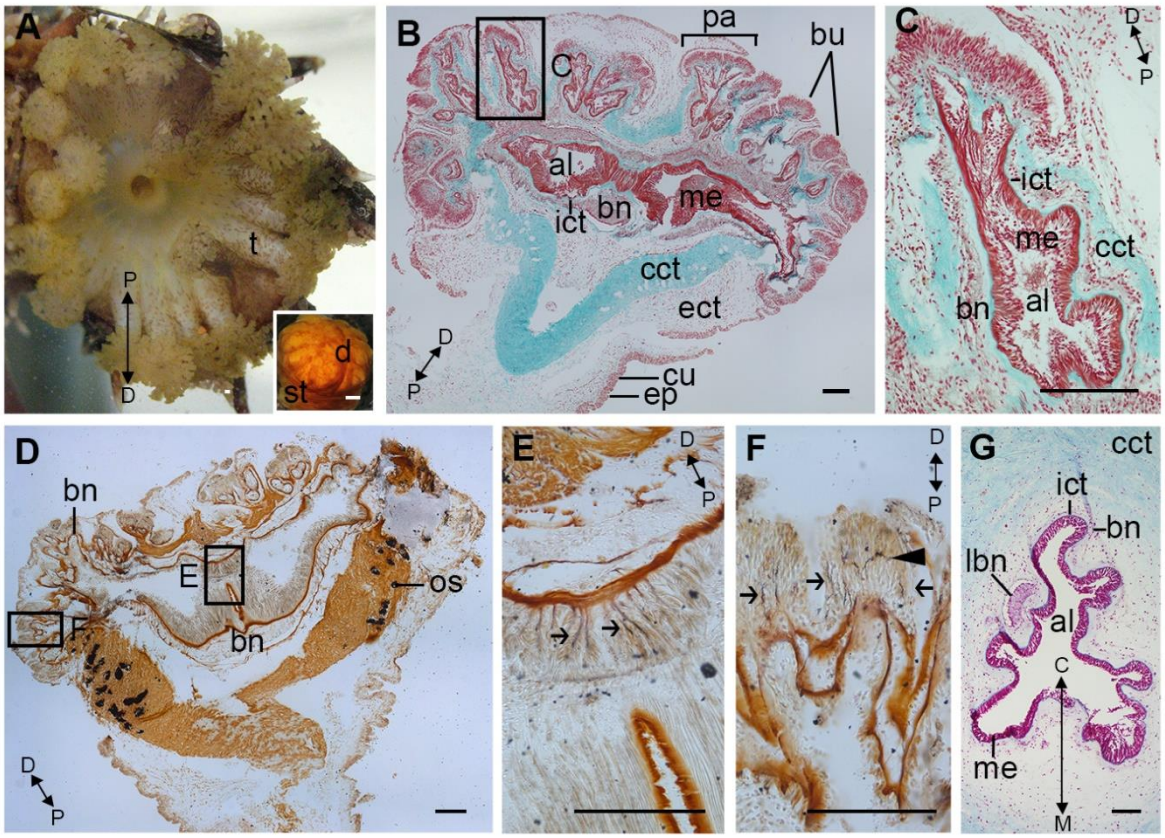


**Figure 2.** Histology of the tentacle. **A** Macroscopic photograph of the oral cavity showing the crown of tentacles (*t*) surrounding the mouth. **Insert** Each tentacle was composed of a stem (*st*) and a distal disc (*d*). **B-D** Longitudinal section through the tentacle stained with Masson's trichrome (B-C) showing the external (*ect*), central (*cct*) and inner (*ict*) connective tissue in *green*, the mesothelium (*me*) in *red*, and the buccal nerve (*bn*) in *light red*; and stained with Palmgren's stain (D) showing the buccal nerve (*bn*) in *dark brown* and the ossicles (*os*) in *black*. **E - F** Higher magnification (E) of the centre of the stem where nerves stained in *black* are seen in the mesothelium (arrows) and, (F) in the bud where apical neurites (arrows) project from the nerve plate (arrowhead) into the epidermis. **G** Transverse section of the tentacle stem stained with Miligan's Trichrome showing the longitudinal buccal nerve (*lbn*) and the buccal nerve plexus (*bn*) in *light purple*, the mesothelium (*me*) in *magenta* and the connective tissue (*ict*: internal connective tissue, *cct*: central connective tissue) in *blue*. *al*: ambulacral lumen, *bu*: bud, *cu*: cuticle, *pa*: papilla. D, P (in A, B, C, E, F) and C, M (in G) indicate respectively, distal, proximal, central and marginal orientations. Scale bars: 100 µm.

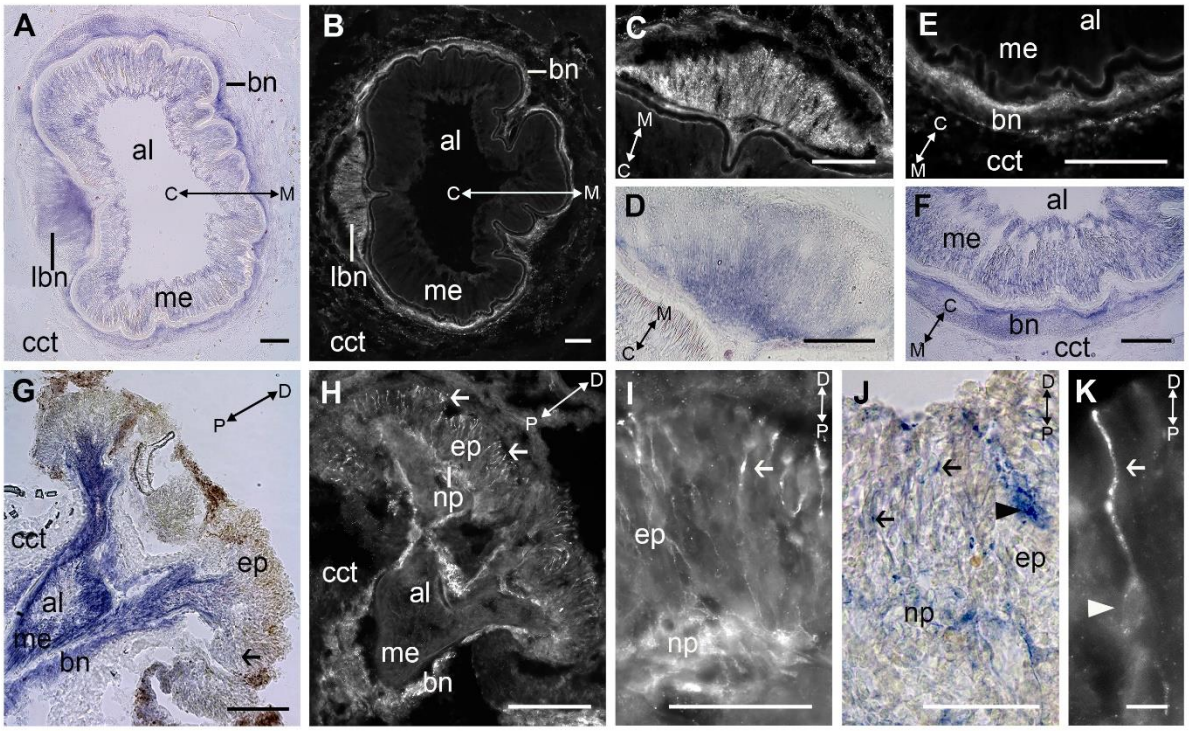


**Figure 3.** NADPH-d histochemistry and NOS immunohistochemistry of the tentacle. **A-B** Transverse section of the stem of the tentacle showing a strong positive histochemical reaction for NADPH-d (A) and immunoreactivity with anti-NOS antibodies (B) in the buccal nerve (*bn*) and the longitudinal buccal nerve (*lbn*), and a less intense signal for both markers in the mesothelium (*me*). **C – F** Higher power magnification of the longitudinal buccal nerve (C-D) and, the buccal nerve and mesothelium (E-F) showing anti-NOS (C, E) and NADPH-d (D, F) reactivity. **G - H** The papilla of a tentacle where NADPH-d reactivity (G) and anti-NOS immunoreactivity (H) were strong in the buccal nerve and less intense in the mesothelium, and where fibres reactive with both markers (NADPH-d and anti-NOS, arrows) were seen in the epidermis (*ep*) of the two buds. **I - K** Higher magnification of the epidermis of a tentacle bud showing fibres (arrows) immunoreactive with anti-NOS (I, K) and NADPH-d (J) in the extremity of the bud as well as in the nerve plate (*np*), with some cell-bodies reactive with both markers (arrowheads). *cct*: central connective tissue. C, M (in A, B, C, D, E, F) and P, D (in G, H, I, J, K) indicate respectively, central, marginal, proximal and distal orientations. Scale bars: 100 µm in A– H, 25 µm in I – J and 5 µm in K.

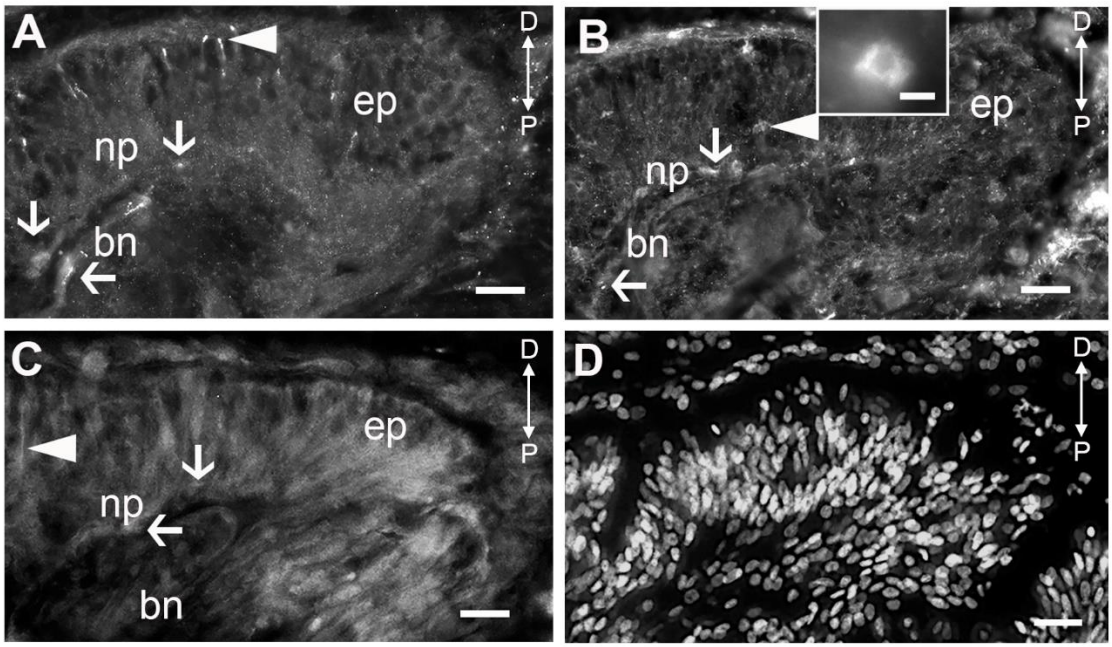


**Figure 4.** Comparison of anti-NOS, anti-serotonin and anti-tubulin immunoreactivity in the tentacle disc. **A** Nitrergic fibres found in the upper area in contact with the environment (arrowhead), in the buccal nerve (*bn*; horizontal arrow) and in the nerve plate (*np*; vertical arrows). **B** Serotonin positive cell bodies (arrowhead; insert) in the epidermal cells and immunoreactive fibres were also identified in the nerve plate (vertical arrow) and the buccal nerve (horizontal arrows). **C** Tubulin positive immunofluorescence in the buccal nerve plexus (horizontal arrow), in some fibres in the nerve plate (vertical arrow) and within the cell clusters (arrowhead). **D** DAPI-stained section showing the distribution of cells within the bud. *ep*: epidermis. D and P in all panels indicate distal and proximal orientations. Scale bars: 25 µm and in all inserts: 5 µm.

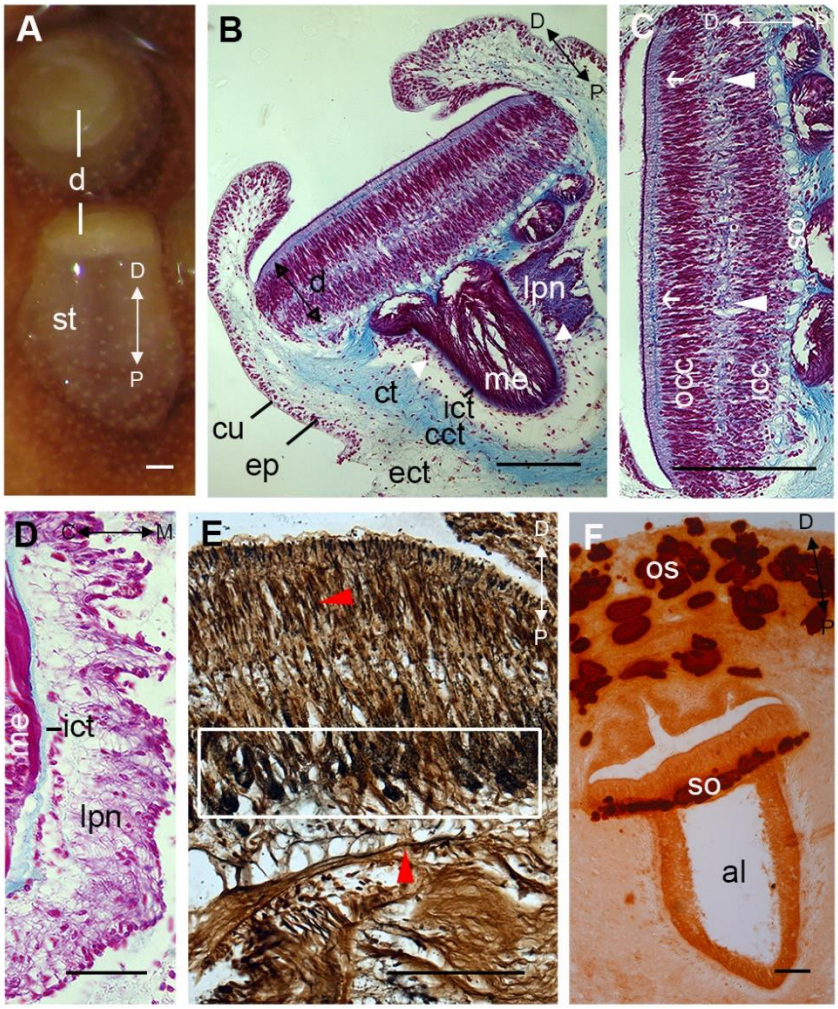


**Figure 5.** Histology of the tube feet. **A** Macroscopic photograph of the podia showing the stem (*st*) and the distal disc (*d*) from the ventral side. **B** Longitudinal section of the podia stained with Milligan's Trichrome showing the tissue layer subdivision: cuticle (*cu*), epidermis (*ep*), connective tissue (*ct*) in *blue* (external connective tissue, *ect*; central connective tissue, *cct;* internal connective tissue, *ict*), longitudinal podial nerve (*lpn*) and podial nerve plexus (arrowheads) in *light purple*, and mesothelium (*me*) in *magenta.* **C** Higher magnification of the terminal disc on the tube feet showing the inner (*icc*) and outer (*occ*) clusters of cells, surrounded by the connective tissue above the occ (arrows) and between them (arrowheads). **D - E** Higher magnification of the longitudinal podial nerve stained with Milligan's Trichrome (D) and of the upper part of the tube feet stained with Palmgren's (E) showing the heavily stained nerve fibres (red arrowheads). The white rectangle indicates the black deposits corresponding to the calcified ossicles. **F** Alizarin red staining showing the ossicles (*os*) and the supporting ossicles (*so*). D, P (in A, B, C, E, F) and C, M (in D) indicate respectively, distal, proximal, central and marginal orientations. Scale bars: 100 µm.

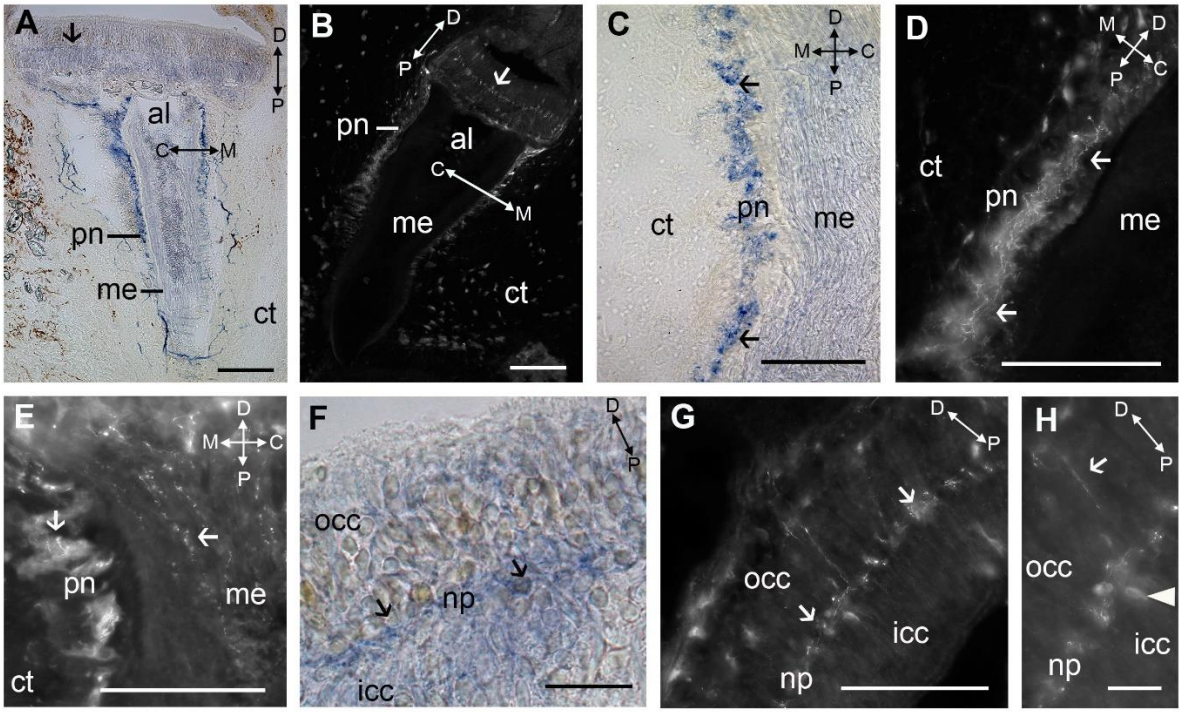


**Figure 6.** NADPH-d histochemistry and NOS immunohistochemistry of the tube feet. **A – B** Positive histochemical reaction to NADPH-d (A) and immunoreactivity to anti-NOS (B) in the stem highlighting the podial nerve plexus (*pn*) extending into the mesothelium (*me*) and connective tissue (*ct*) and in the nerve plate of the distal disc (arrows). **C – E** Higher magnification of the stem showing fibres (arrows) reactive with NADPH-d (C) and anti-NOS (D) in the podial nerve, and in the mesothelium (E). **F – H** Higher magnification of the distal disc showing fibres reactive to NADPH-d (F) and anti-NOS (G) in the nerve plate (arrows), and highlighting the presence of cell bodies immunoreactive with anti-NOS in the cell clusters of the disc (arrowhead) (H). D, P (in A, B, C, D, E, F, G, H) and C, M (in A, B, C, D, E) indicate respectively, distal, proximal, central and marginal orientations. Scale bars: A – E and G:100 µm and F, H: 20 µm.

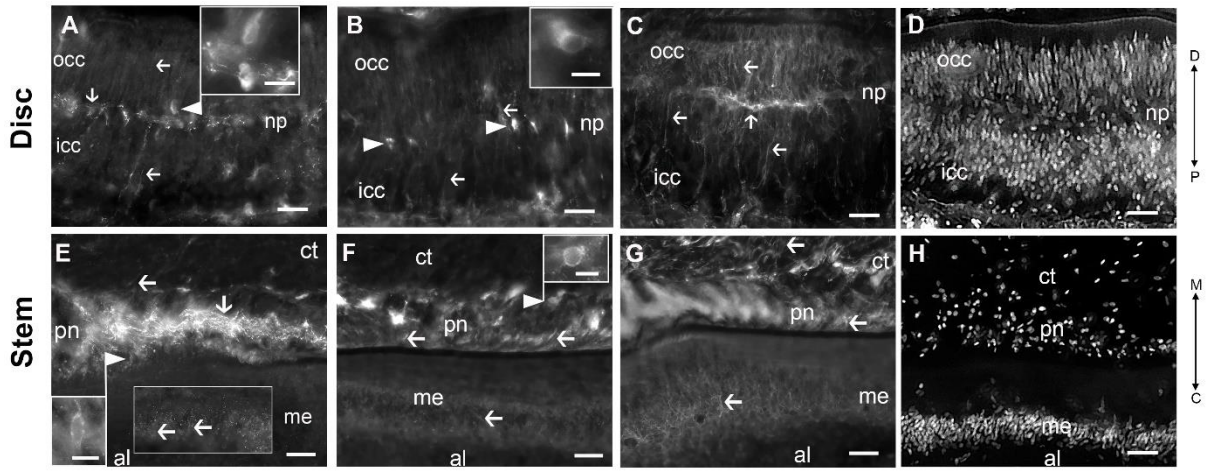


**Figure 7.** Comparison of anti-NOS, anti-serotonin and anti-tubulin immunoreactivity in the tube feet disc and stem. **A – D** Tube feet disc. **A** Nitrergic fibres coming from the nerve plate are seen in both cell clusters (horizontal arrows; outer cluster of cell, *occ*; inner cluster of cells, *icc*) and a few cell bodies immunopositive with anti-NOS (arrowhead; insert) could be found in proximity to the nerve plate (*np*). **B** Serotonin immunoreactivity is present in fibres projecting from the nerve plate and in cell clusters (arrows). A few serotonin immunoreactive cell bodies are present around the nerve plate (arrowheads; insert). **C** Fibres immunopositive with anti-tubulin are present in the nerve plate (vertical arrow) and between the nerve plate and the two cell clusters (horizontal arrows). **D** DAPI-stained section showing the nuclei of the densely packed outer cell cluster and the loosely packed inner cell cluster. **E – H** Tube feet stem. The same general tissue organization was observed in the stem of the papillae and the tentacle. **E** An abundance of NOS-immunopositive nitrergic fibres are present in the podial nerve plexus (*pn*) (vertical arrow) compared to the connective tissue (*ct*) and the mesothelium (*me*) (horizontal arrows). Only a few nitrergic cell bodies were found in the podial nerve plexus (arrowhead; insert). **F** Serotonin-immunopositive cell bodies (arrowhead; insert) in the podial nerve plexus, and fibres (arrows) in both the podial nerve plexus and mesothelium. **G** Strong immunoreactivity to anti-tubulin in the podial nerve plexus, the mesothelium and connective tissue (fibres: arrows). **H** DAPI-stained section indicating the main structures: connective tissue (*ct*), podial nerve plexus (*pn*) and mesothelium (*me*). al: ambulacral lumen. D, P (in A, B, C, D) and C, M (in E, F, G, H) indicate respectively, distal, proximal, central and marginal orientations. Scale bars: 25 µm and in all inserts: 5 µm.

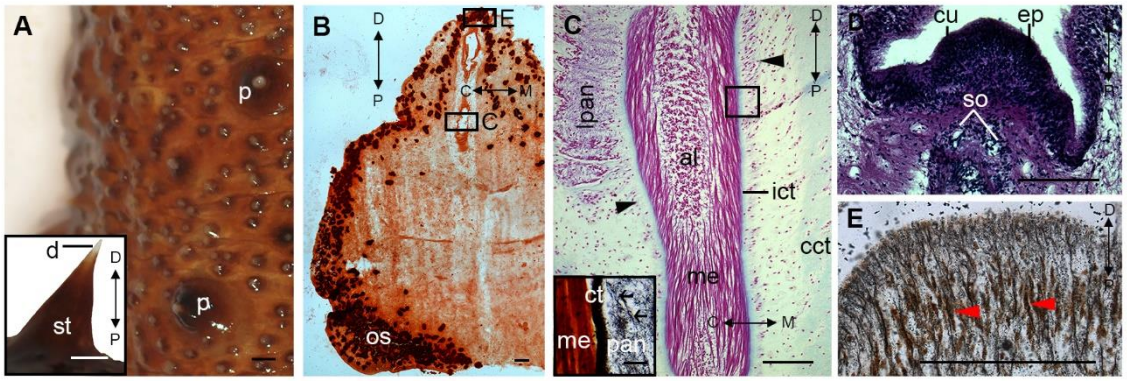


**Figure 8.** Histology of the papillae. **A** Macroscopic photograph of the dorsal side showing two papillae and (*insert*) a higher magnification of a papillae showing the stem (*st*) and the white distal disc (*d*). **B** Distribution of the ossicles (*os*) in the papillae. The boxed regions in A and B are shown in higher magnification in photographs C and E. **C** Higher magnification of the stem stained with Milligan's trichrome clearly showing the connective tissue (*ict:* internal and *cct:* central) in *blue*, the longitudinal papillae nerve (*lpan*) and papillae nerve plexus (arrowheads) in *light purple*, the mesothelium (*me*) in *magenta* and the ambulacral lumen (*al*); with (*insert*) Palmgren's staining showing nervous fibres in the papillae nerve plexus (*pan*) in *black* (arrows). **D – E** Higher magnification of the distal disc stained with (D) H&E and (E) Palmgren's showing the nerve fibres (arrowheads) in *black.* D, P (in A, B, C, D, E) and C, M (in B, C) indicate respectively, distal, proximal, central and marginal orientations. Scale bars: A: 500 µm, B, D, E: 100 µm and C in insert 25 µm.

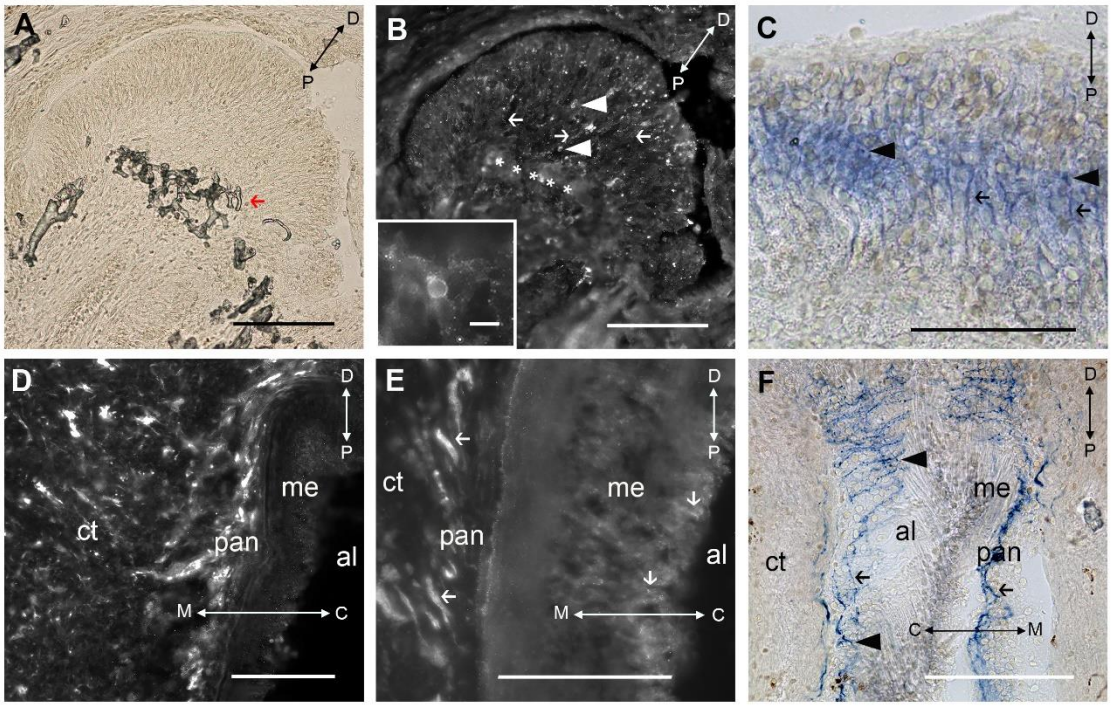


**Figure 9.** NADPH-d histochemistry and NOS immunohistochemistry of the papillae. **A** Section under bright field light of the terminal part of the papillae showing the localization of the ossicles (arrow). **B – C** Positive NOS-immunoreactivity (B; asterisks localize the ossicles) and NADPH-d staining (C) in the terminal part of the papillae showing some nitrergic fibres (arrows) and cell bodies (arrowheads), with a higher magnification of a nitrergic cell body presented in the insert in B. **D** – **F** Stem of the papillae showing strong NOS-immunoreactivity (D, E) and NADPH-d (F) in the papillae nerve (*pan*), with a weaker signal in the mesothelium (*me*) (fibres: arrows and cell bodies: arrowheads). *al*: ambulacral lumen, *ct*: connective tissue. D, P (in all panels) and M, C (in D, E, F) indicate respectively, distal, proximal, marginal and central orientations. Scale bars: 100 µm in all figures; insert in B: 10 µm.

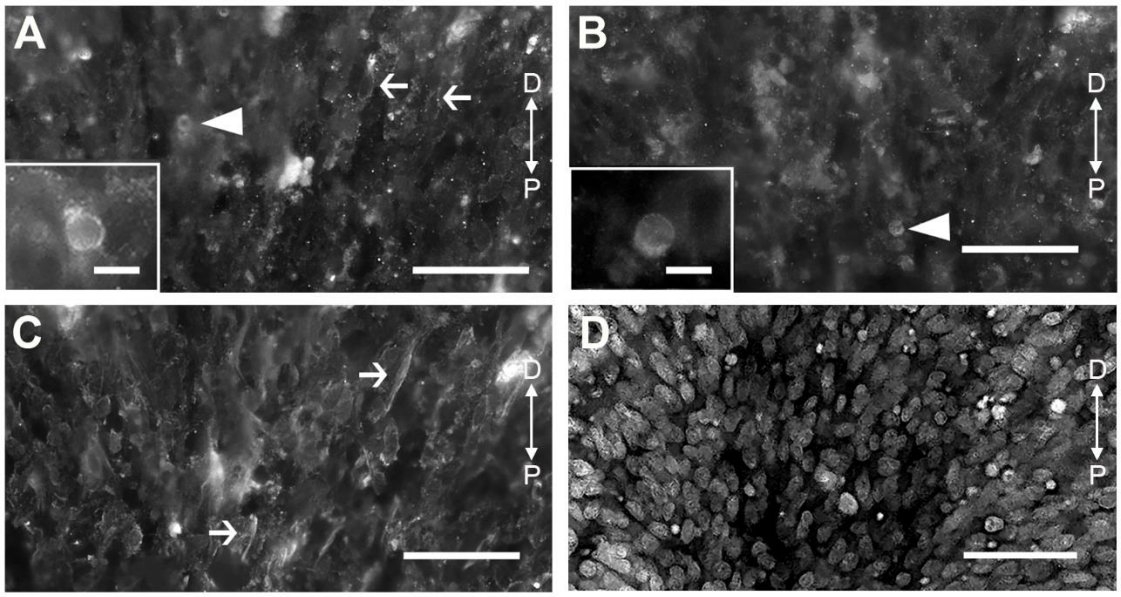


**Figure 10.** Comparison of anti-NOS, anti-serotonin and anti-tubulin immunoreactivity in the terminal end of a papillae. **A** Immunoreactive nitrergic fibres (arrows) and cell bodies (arrowhead; insert), and **B** immunoreactive serotonin cell bodies (arrowhead; insert) could be seen in the epidermal cells. **C** Tubulin immunofluorescence in fibres (arrows) and **D** DAPI-stained sections show the abundance of nuclei in the terminal disc of the papillae. D and P in all panels indicate distal and proximal orientations. Scale bars: 25 µm and all inserts: 5 µm.

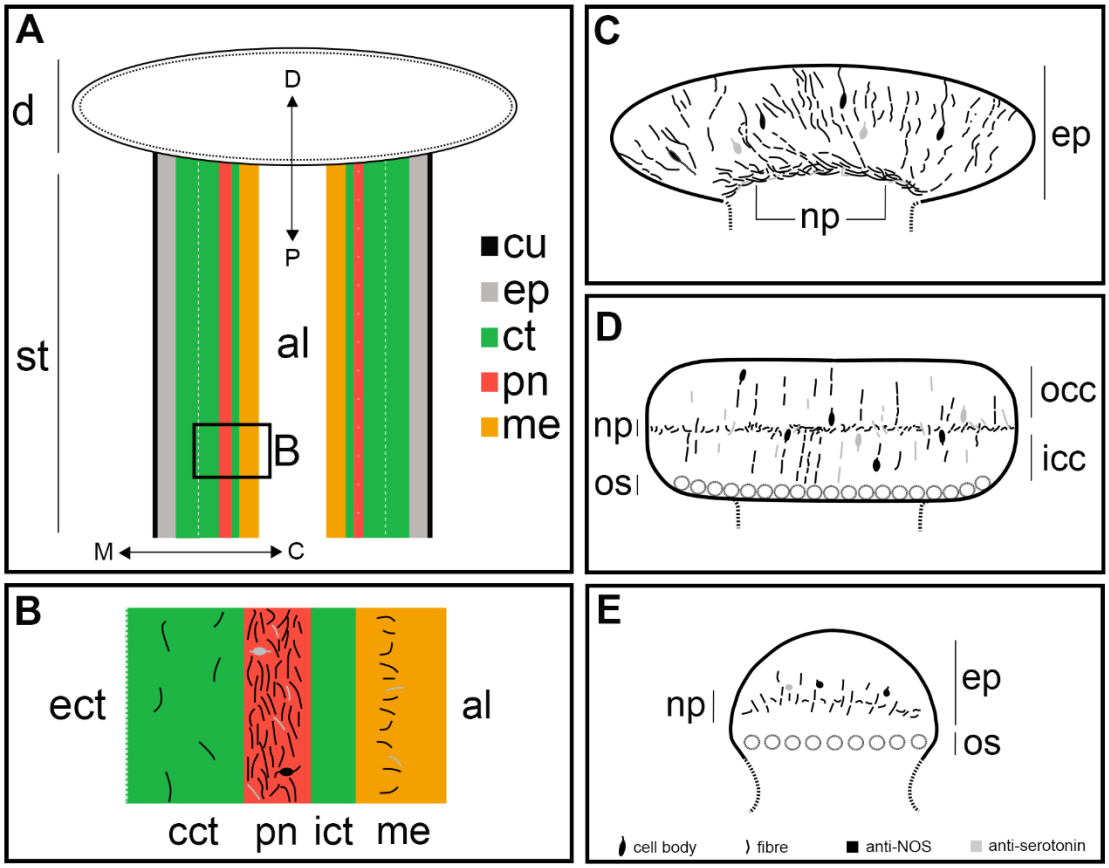


**Figure 11.** Schematic diagrams of the holothurian podia. **A** Longitudinal representation of a podia's stem showing the disc (*d*) and the stem (*st*) containing the following layers: cuticle (*cu*) in *black*, epidermis (*ep*) in *grey*, connective tissue (*ct*) in *green*, podial nerve (*pn*) in *red* and mesothelium (*me*) in *orange*. D, P, M, and C indicate distal, proximal, marginal and central orientations, respectively. **B** Higher magnification of the stem tissue layers where the distribution of fibres and cell bodies labelled with anti-NOS (*black*) and anti-serotonin (*grey*) are schematically represented in the central connective tissue (*cct*), podial nerve (*pn*), internal connective tissue (*ict*) and mesothelium (*me*). **C – E** Higher magnification of the three types of holothurian's disc where the distribution of fibres and cell bodies labelled with anti-NOS (*black*) and anti-serotonin (*grey*) are schematically represented in the tentacle (C), tube feet (D) and papillae (E). *ep*: epidermis, *icc*: inner cluster of cells, *np*: nerve plate, *occ*: outer cluster of cells, *os*: ossicles.

# Localization and distribution of nitric oxide synthase and other neuronal markers in the podia of *Holothuria arguinensis.*

**Nathalie Marquet[#], Adelino V.M. Canário and Deborah M. Power**

CCMAR Centre of Marine Sciences, University of Algarve, Campus de Gambelas, 8005-139 Faro, Portugal

[#] Corresponding author: N. Marquet

e-mail: nmarquet@gmail.com

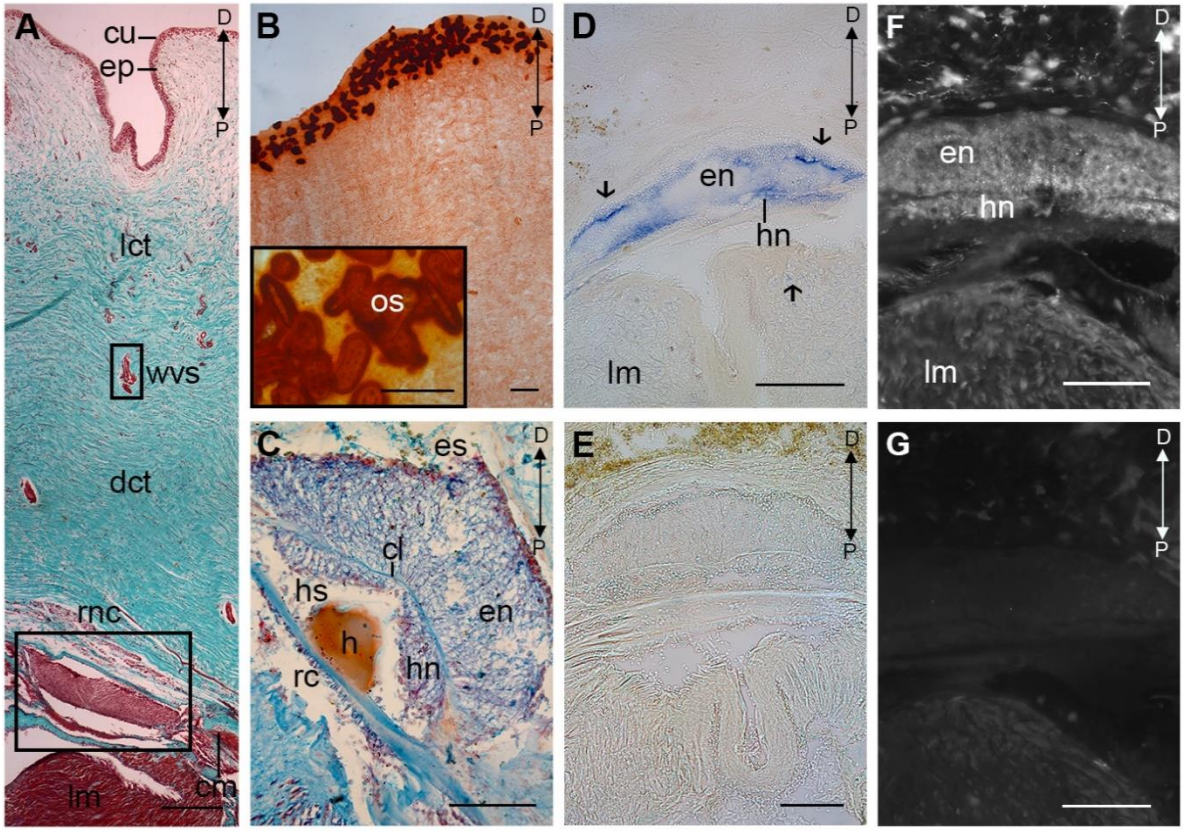


**Figure S1.** Histology, NADPH-histochemistry and NOS immunohistochemistry of the body wall including the radial nerve cord (RNC). **A** Transverse section through the body wall stained with Masson's Trichrome showing the loose (*lct*) and dense (*dct*) connective tissue *in green*, the radial nerve cord (*rnc*) in *dark pink*, the circular (*cm*) and longitudinal (*lm*) muscles in *red*. **B** Surface part of the body wall showing the distribution of the ossicles and (insert) typical ossicles (*os*) stained with Alizarin red. **C** Deeper part of the body wall highlighting the radial nerve cord stained with Milligan's Trichrome. **D – E** Positive histochemical reaction for NADPH-d in the RNC (D) and absence of reactivity in the control (E). **F – G** Immunopositivity to anti-NOS (F) in the RNC and the absence of signal in the control (G). *cu*: cuticle, *cl*: connective tissue layer, *es*: epineural sinus, *en*: ectoneural neuroepithelium, *ep*: epidermis, *h*: haemal lacuna, *hs*: hyponeural sinus, *hn*: hyponeural neuroepithelium, *rnc:* radial nerve cord, *wvs*: water vascular canal. D, P (in all panels) indicate distal and proximal orientations. Scale bars: 100 µm.

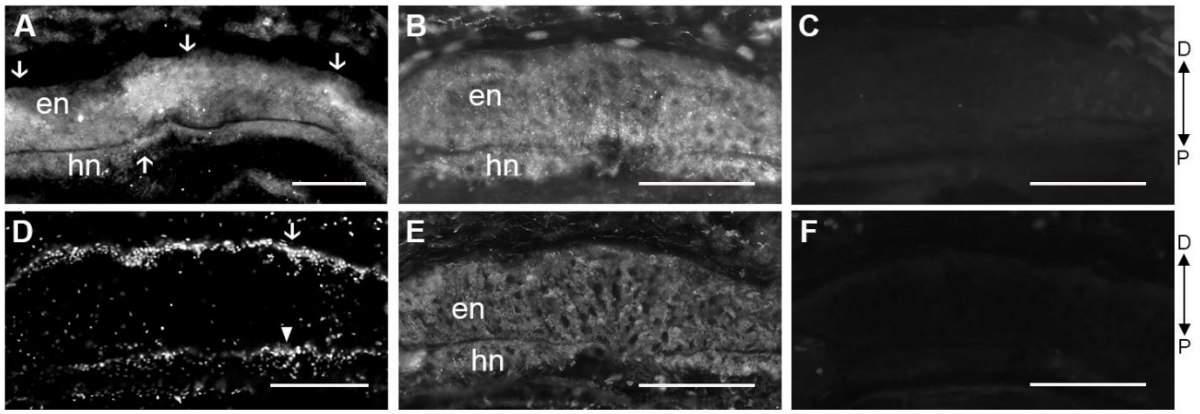


**Figure S2.** Immunohistochemistry of the radial nerve cord. **A** Serotonin immunolabeling is mainly distributed in the central and lateral region of the ectoneural (*en*) part of the RNC and in the central region of the hyponeural (*hn*) part of the RNC. **B** An extensive positive reaction to anti-NOS is present in both parts of the RNC. **C** Control slide where only the secondary anti-rabbit antibody was applied. **D** DAPI-stained section showing the abundance of cell nuclei lining the ectoneural (arrow) and hyponeural (arrowhead) components of the RNC, and the region with relatively lower abundance of cell nuclei within the RCN. **E** Tubulin immunoreactivity is largely distributed in both parts of the RNC. **F** Control slide where only the secondary anti-mouse antibody was applied. D, P (in all panels) indicate distal and proximal orientations. Scale bars: 100 µm.

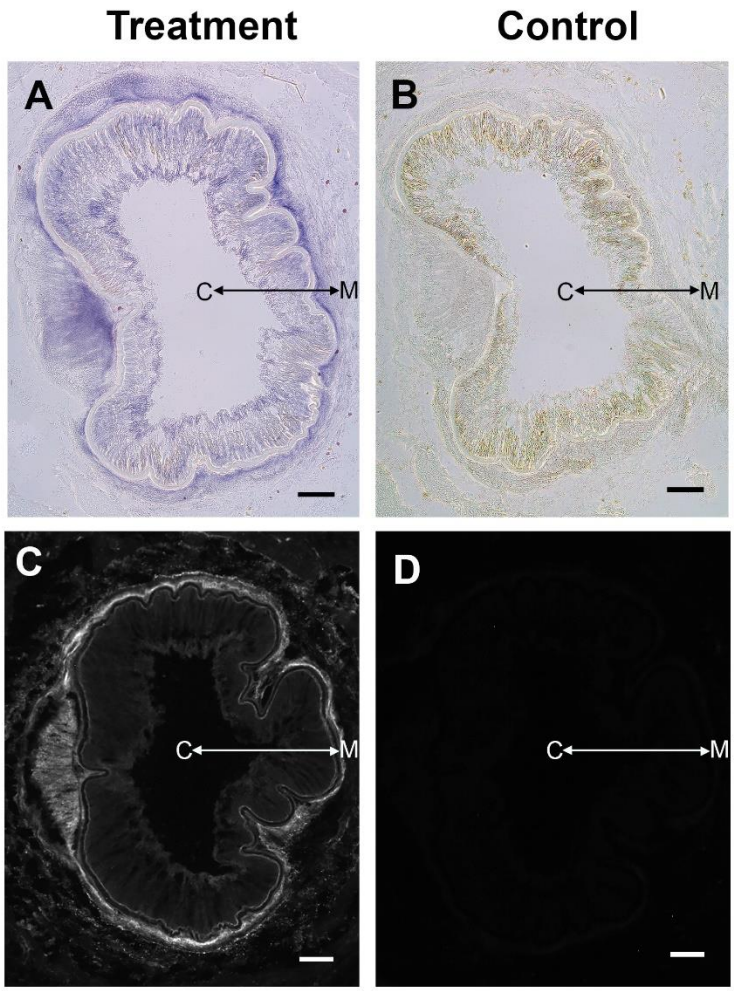


**Figure S3.** Treatment (NADPH-d and anti-NOS) (A, C) and control (B, D) slides in the stem of the tentacle. **A – B** Reactivity to NADPH-d in the treatment section (A) and absence of reactivity in the control (B). **C – D** Immunopositivity to anti-NOS in the treatment section (C) and control where anti-NOS was omitted (D). C, M (in all panels) indicate central and marginal orientations. Scale bars: 100 µm.

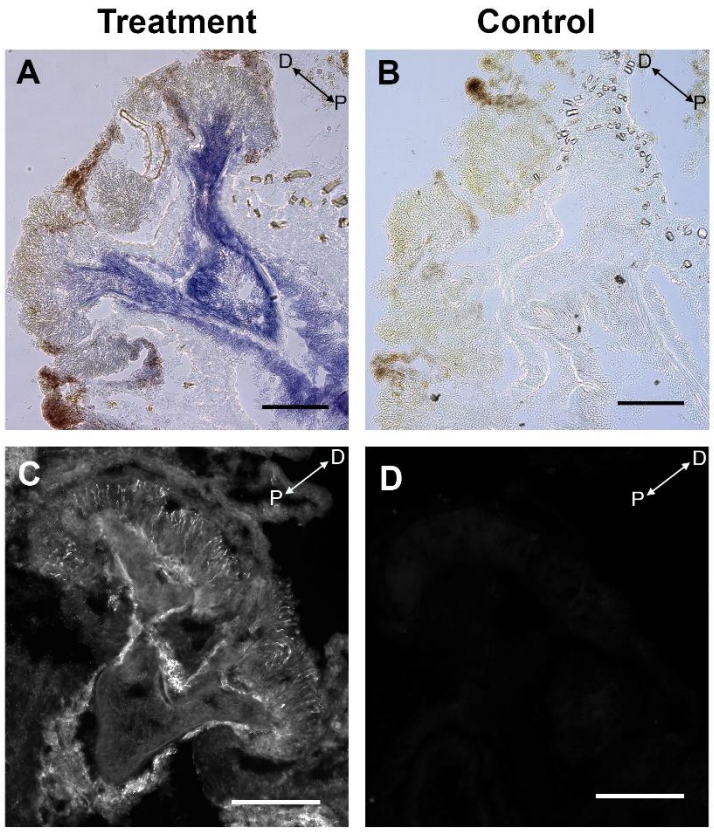


**Figure S4.** Treatment (NADPH-d and anti-NOS) (A, C) and control (B, D) slides in a bud of the tentacle. **A – B** Reactivity to NADPH-d in the treatment section (A) and absence of reactivity in the control (B). **C – D** Immunopositivity to anti-NOS in the treatment section (C) and control where anti-NOS was omitted (D). P, D (in all panels) indicate proximal and distal orientations. Scale bars: 100 µm.

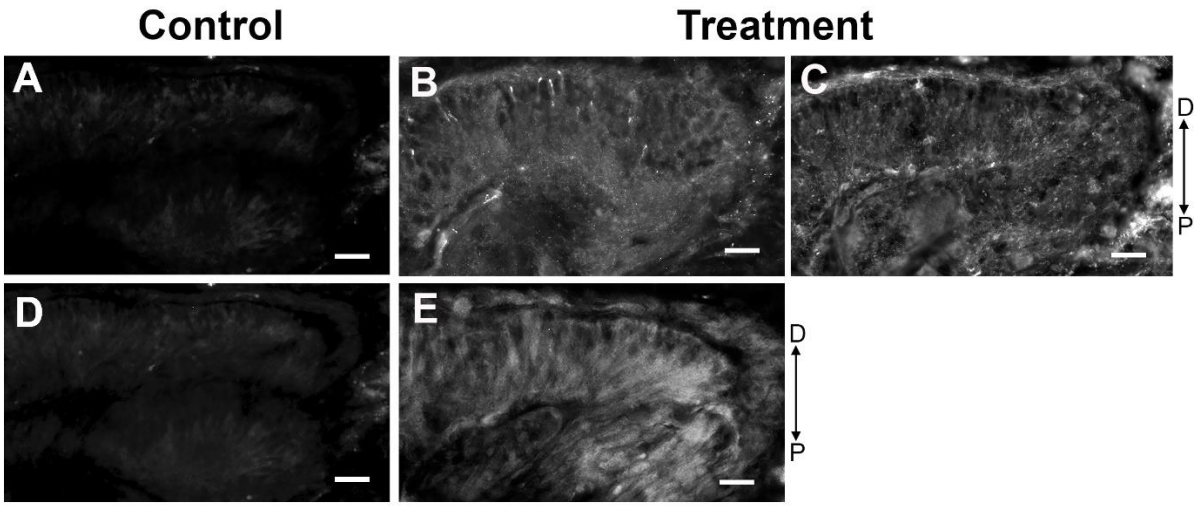


**Figure S5.** Treatment (B, C, E) and control (A, D) slides in the disc of the tentacle. **A** Control slide where only the secondary anti-rabbit antibody was applied and **B – C** the treatment slides using the same secondary antibody with (B) anti-NOS and (C) anti-serotonin. **D** Control slide where anti-tubulin was omitted and only the secondary anti-mouse antibody was applied and **E** a section with the anti-tubulin primary antibody and the anti-mouse secondary antibody. P, D (in all panels) indicate proximal and distal orientations. Scale bars: 25µm.

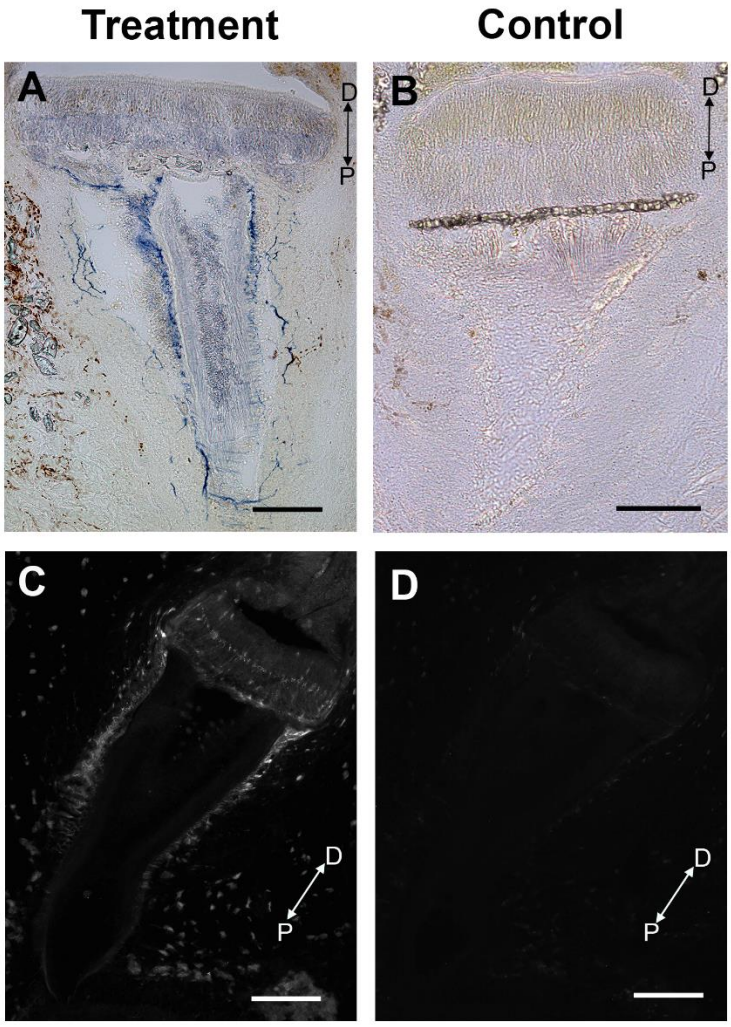


**Figure S6.** Treatment (NADPH-d and anti-NOS) (A, C) and control (B, D) slides in the tube feet. **A – B** Reactivity to NADPH-d in the treatment slide (A) and absence of reactivity in the control slide (B). **C – D** Immunoreactivity to anti-NOS in the treatment slide (C) and control slide where anti-NOS was omitted (D). P, D (in all panels) indicate proximal and distal orientations. Scale bars: 100 µm.

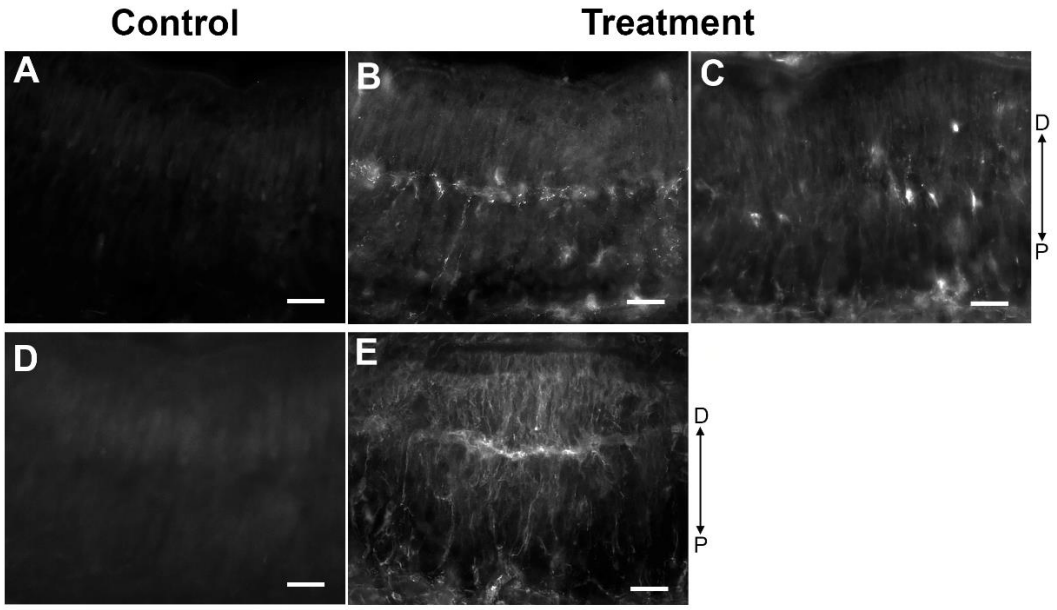


**Figure S7.** Treatment (B, C, E) and control (A, D) slides in the disc of the tube feet. **A** Control section where only the secondary anti-rabbit antibody was applied, and **B** anti-NOS and **C** anti-serotonin primary antisera was used with the anti-rabbit secondary antibody. **D** Control where only the secondary anti-mouse antibody was applied and **E** the treatment section using anti-tubulin and anti-mouse secondary antibody. P, D (in all panels) indicate proximal and distal orientations. Scale bars: 25µm.

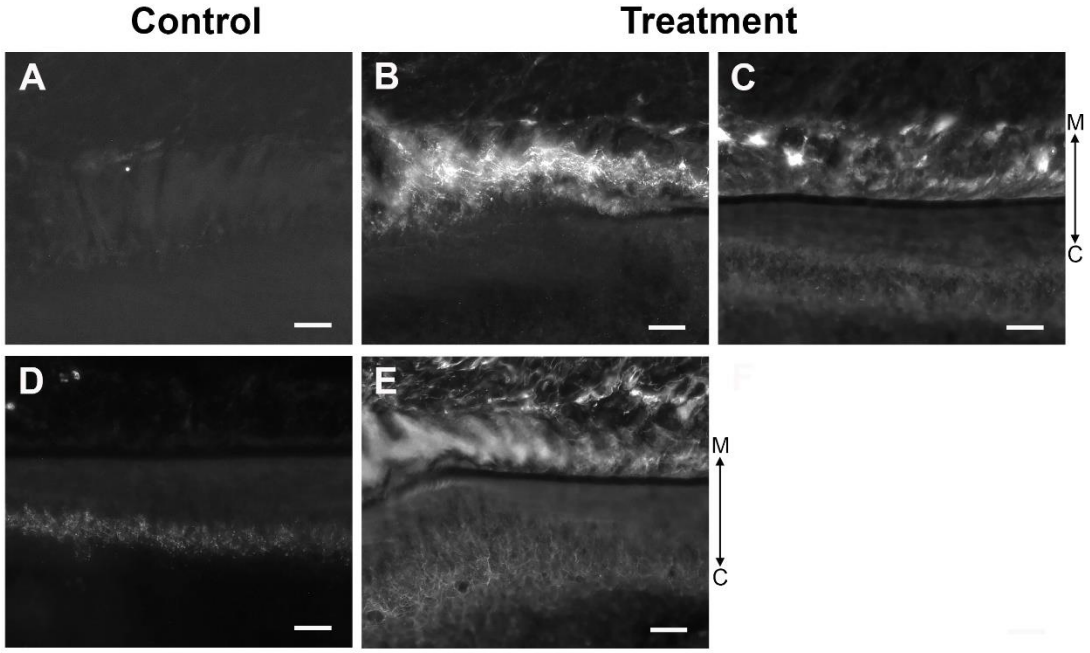


**Figure S8.** Treatment (B, C, E) and control (A, D) sections in the stem of the tube feet. **A** Control section where only the secondary anti-rabbit antibody was applied and **B** anti-NOS and **C** anti-serotonin primary antisera with the anti-rabbit secondary antibody. **D** Control sections where only the secondary anti-mouse antibody was applied and **E** the treatment sections using anti-tubulin and anti-mouse secondary antibody. C, M (in all panels) indicate central and marginal orientations. Scale bars: 25µm.

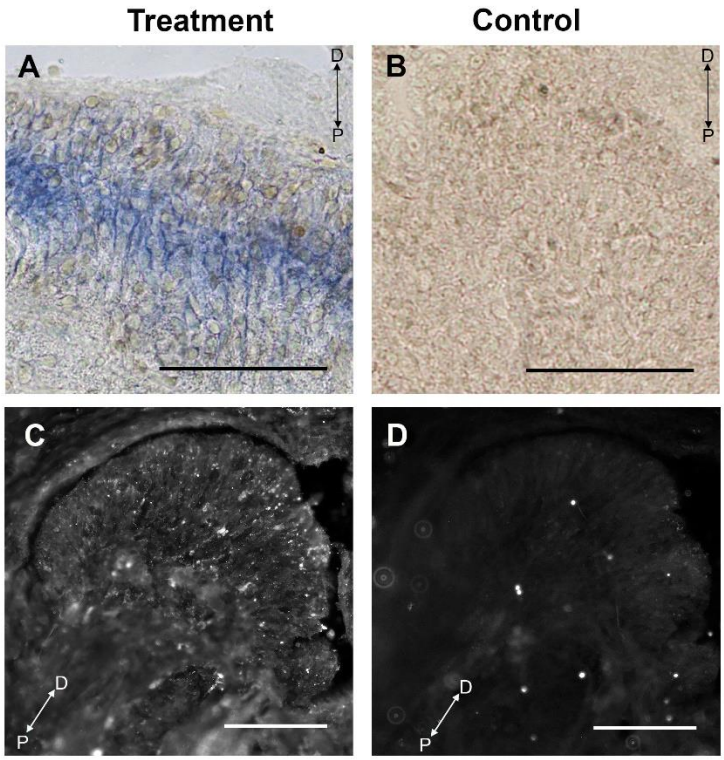


**Figure S9.** Treatment (NADPH-d and anti-NOS) (A, C) and control (B, D) in the pointed structure of the papillae. **A** Reactivity to NADPH-d in the treatment section and **B** absence of reactivity in the control. **C** Immunoreactivity to anti-NOS in the treatment section and **D** control. P, D (in all panels) indicate proximal and distal orientations. Scale bars: 50 µm in A, B and 100 µm in C, D.

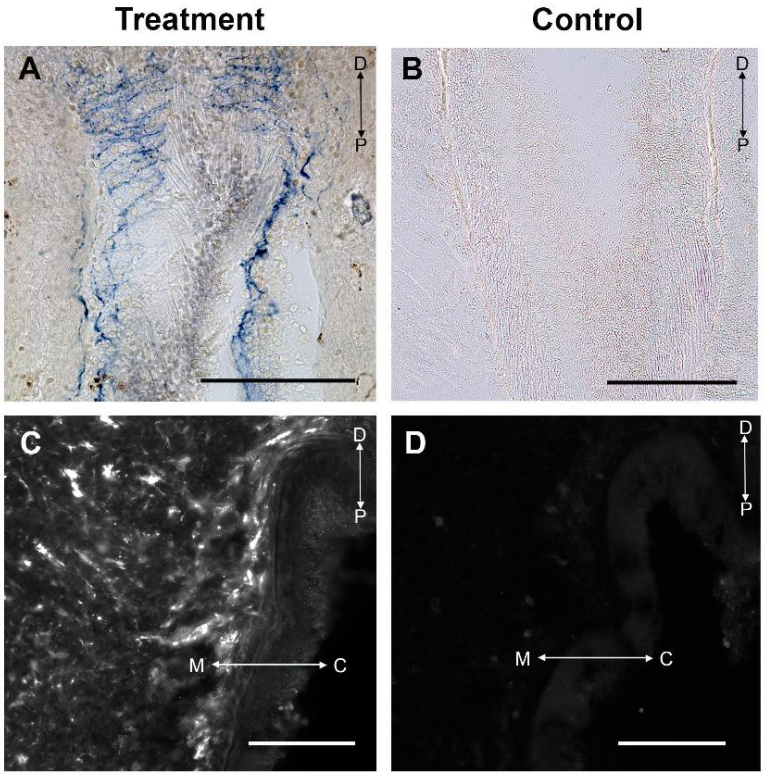


**Figure S10.** Treatment (NADPH-d and anti-NOS) (A, C) and control (B, D) in the stem of the papillae. **A** Reactivity to NADPH-d in the treatment section and **B** absence of reactivity in the control. **C** Immunoreactivity to anti-NOS in the treatment section and **D** control. P, D (in all panels) and C, M (in C, D) indicate respectively, proximal, distal, central and marginal orientations. Scale bars: 100 µm.

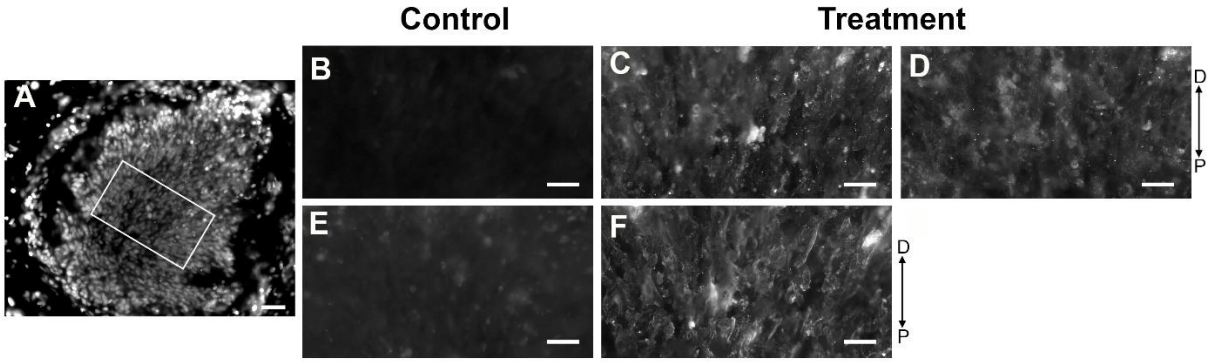


**Figure S11.** Treatment (A, C, D, F) and control (B, E) in the pointed structure of the papillae. **A** Section stained with nuclear staining DAPI in which the white rectangle delineates the area of the papillae shown in the treatment sections. **B** Control where only the secondary anti-rabbit antibody was applied and the treatment slides **C** anti-NOS and **D** anti-serotonin using the anti-rabbit secondary antibody. **E** Control where only the secondary anti-mouse antibody was applied and the treatment section **F** with anti-tubulin and anti-mouse secondary antibody. P, D (in all panels) indicate proximal and distal orientations. Scale bars: 25µm.